The University of Alberta
Printing Department
Edmonton, Alberta

THE UNIVERSITY OF ALBERTA

ANELASTIC BEHAVIOR OF IRON AT LOW TEMPERATURES

BY

LEONARD ARTHUR VIENNEAU

A THESIS

SUBMITTED TO THE FACULTY OF GRADUATE STUDIES IN

PARTIAL FULFILLMENT OF THE REQUIREMENTS FOR THE

DEGREE OF MASTER OF SCIENCE

DEPARTMENT OF PHYSICS

EDMONTON, ALBERTA

JANUARY, 1968

UNIVERSITY OF ALBERTA

FACULTY OF GRADUATE STUDIES

The undersigned certify that they have read and recommend to the Faculty of Graduate Studies for acceptance, a thesis entitled "ANELASTIC BEHAVIOR OF IRON AT LOW TEMPERATURES", submitted by Leonard Arthur Vienneau in partial fulfilment of the requirements for the degree of Master of Science.

ABSTRACT

In order to maintain the amplitude of mechanical vibrations in a solid constant, it is necessary to supply energy to the system. This dissipation of energy may occur via many distinct mechanisms.

The present work was an experimental study carried out in order to determine the mechanism which causes the anomalously large dissipation observed in iron, at low temperatures for vibration frequencies in the KH_z range, by Bruner (1960), Heller (1961) and Verdini (1962). It will be shown that it is possible to explain this behavior as being due to the damping of dislocations by the conduction electrons in the metal, assuming a dislocation density of 10^7 cm^{-2} and an average length for these dislocations of 4.3×10^{-5} cm. These values are in good agreement with those found by other techniques.

In the course of this work, the damping of vibrations was measured in two other ferromagnetic metals, cobalt and nickel. The results for cobalt showed evidence of the unstable hexagonal phase of this metal which has previously been seen by other methods (Bozorth, 1951)

ACKNOWLEDGEMENTS

I wish to express my gratitude to Dr. L. Verdini, my research supervisor, both for suggesting this project and for his patient encouragement and guidance throughout the course of this work.

I am also indebted to the technical staff of the Physics Department for their assistance during this project.

It is a pleasure to acknowledge the financial support of both the Physics Department and the National Research Council during this work.

TABLE OF CONTENTS

LIST OF FIGURES

CHAPTER I

INTRODUCTION

In an ideal elastic solid Hooke's law is obeyed, that is each stress component is a linear real function of the strain components alone. Within this law, there is no allowance for damping of vibrations or traveling waves. In a real solid, however, vibrations and waves are attenuated and the relation between stress and strain components, although linear, must contain terms in stress and strain rate (Zener, 1948). This non ideal behavior stems from the fact that phonons, the quanta of vibrational energy, interact with electrons, dislocations, point defects etc., in the solid, which absorb energy in the process giving rise to attenuation. Vibrations in a solid can also set up thermal currents and since this heat flow is resistive, elastic energy is absorbed and this produces still another form of attenuation. Heat plays another role in attenuation in that vibrational phonons can be scattered by thermal phonons. Phonons can also be scattered by grain boundaries in polycrystaline solids. Each of the scattering processes produces attenuation, however they are more or less limited to the megacycle frequency range.

Each of the attenuation processes mentioned above affords a method of experimental study on the parameters involved. For instance it is possible to measure the diffusion constant of point defects such as vacancies, interstitial or substitutional impurities. A study of damping due to dislocations can lead to a value for the height of the Peierls barrier or the binding energy of impurities to dislocations. Measurements of the electron phonon interaction will yield the shape of the Fermi surface of a metal or the energy gap of a superconductor. Comprehensive reviews of the various theories involved and their relation to experiment have been given by Mason (1966) and Bhatia (1967). The method of study usually involves the measurement of the temperature and frequency dependence of the vibration damping and of the elastic modulus.

The present work was a study of the anelastic behavior of polycrystaline iron with emphasis on the low temperature region. The method used was to measure the damping of free vibrations set up in circular plates as a function of several parameters, the most direct of which was temperature. The purpose of the experiment was to investigate and explain the large increase in attenuation at low temperatures observed by Bruner (1960), Heller (1961) and Verdini (1962). Measurements were carried out over the temperature range from 4.2°K

to room temperature at frequencies ranging from 10 KH_z to 170 KH_z. The dependence of the anomalous damping on magnetic field, impurity content, and thermal and mechanical treatment was also studied. The dependence of damping on temperature in cobalt and nickel was also measured so that the behavior in iron could be compared with that of other ferromagnetic metals.

CHAPTER II

BASIC THEORY OF ANELASTICITY

A. Ideal Elasticity

The formulation of the theory of elasticity began with Robert Hooke's law which reads:

$$\vec{F} = M\vec{D} \,, \qquad (2.1)$$

where $\vec{F}$ is a force acting on a body to produce a deformation $\vec{D}$. The proportionality constant M is called the elastic modulus of the body. The formulation however required that the force be applied slowly enough that the whole of the body be aware of its presence. This limitation stems from the fact that a mechanical pulse has a finite velocity namely the speed of sound in the material under consideration. Another fact not taken into account by Hooke's law is that a force suddenly applied to a body may set up vibrations in this body. In order for this law to be valid then, the force must be applied over a time which is longer than the period of the lowest frequency normal mode of the specimen.

Voigt (1910) overcame this difficulty by generalizing Hooke's

law to consider all forces including the rapidly varying ones. To do this one divides the material up into small rectangular parallelepiped volumes as illustrated in figure 2.1, of dimensions dx_1 dx_2, and dx_3 and considers only the forces and deformations in these volumes due to the surrounding material. In the limiting case of dx_i tending to zero, the period of the lowest normal mode will tend to zero and any force applied to the elemental volume will be instantly felt in the form of a deformation. The components of the force per unit area on each face of this volume are called the stress components and are noted σ_{ij}. The indices indicate the face on which the force acts and its component respectively. We now define the strain components ϵ_{ij} as:

$$\epsilon_{ij} = \frac{1}{2}\left[(\partial s_i/\partial x_j) + (\partial s_j/\partial x_i)\right] ,$$

where $s_i(x)$ are the components of the displacement of particles at x. Both σ_{ij} and ϵ_{ij} behave as second rank tensors and Hooke's law can be written as:

$$\sigma_{ij} = c_{ijkl}\epsilon_{kl} , \qquad (2.2)$$

where the coefficients c_{ijkl} are called the elastic constants of the medium.

Figure 2.1

Rectangular parallelepiped portion of a medium with stress components illustrated on one face (after Bhatia 1967).

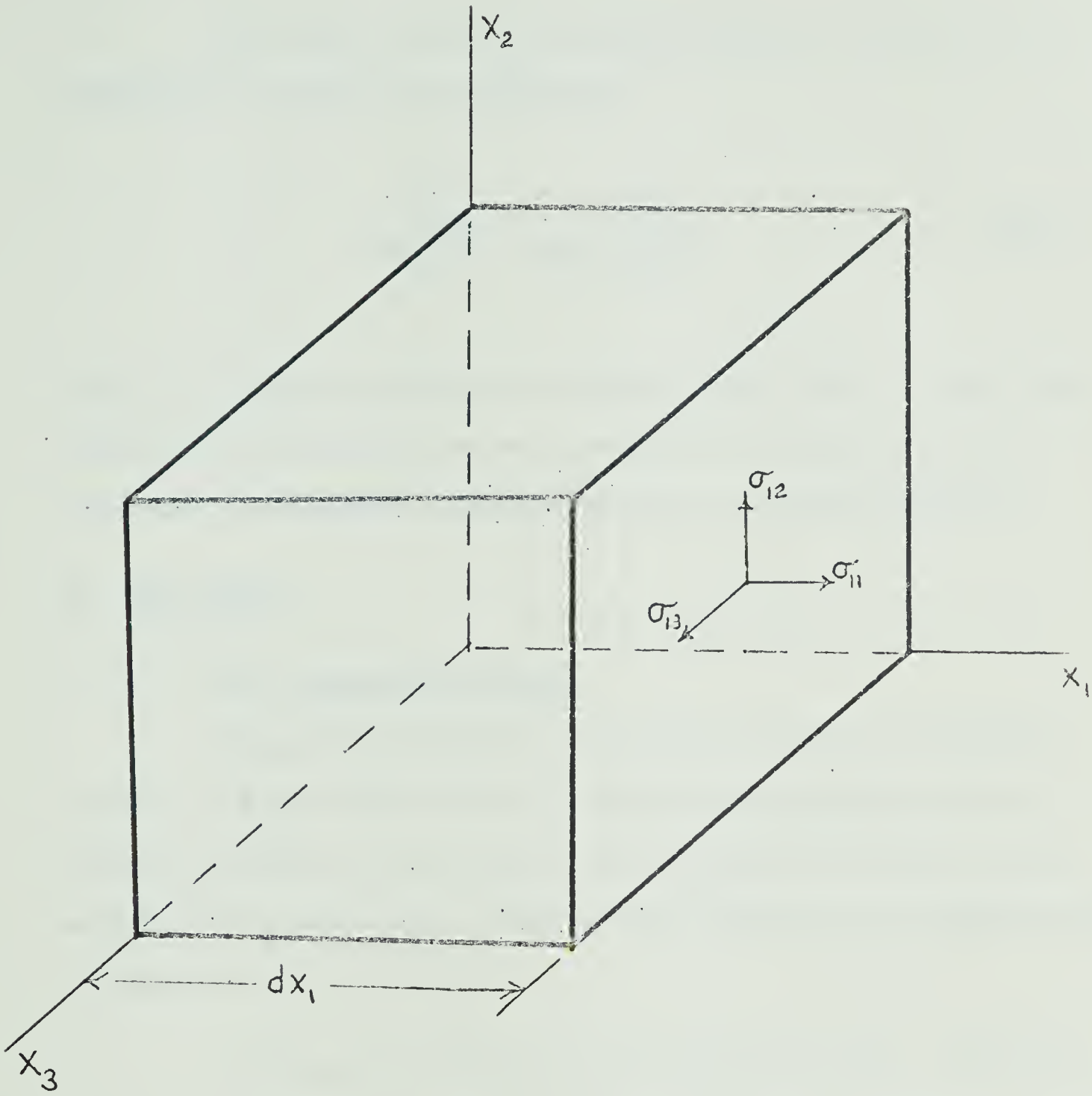
X_2
σ_{12}
σ_{11}
σ_{13}
X_1
dx_1
X_3

With equation (2.2) in mind, the equation of motion of the particles at a point can be written as:

$$\rho_o \frac{\partial^2 s_i}{\partial t^2} = c_{ijkl} \frac{\partial^2 s_k}{\partial x_j \partial x_l} \qquad (2.3)$$

where s_i is again the component of displacement. This is a wave equation and has the usual plane and standing wave solutions and these waves have undiminishing amplitudes in time or distance travelled.

B. Real Solids

(1) Non Elastic Behavior

The solid described by equation (2.2) behaves mechanically as shown in figure 2.2(a) that is a force instantaneously applied at a time t_1 produces an instantaneous deformation which remains constant as long as the force does. The deformation will then go instantaneously to zero when the force does.

A real solid behaves in a very different manner. First of all, the magnitude of the force is limited to what is called the elastic limit. Any force greater than this will produce a permanent deformation in the solid, a phenomenon called plasticity of which no account is

Figure 2.2

The mechanical behavior of (a) the ideal elastic solid and (b) the standard linear solid (Zener, 1948).

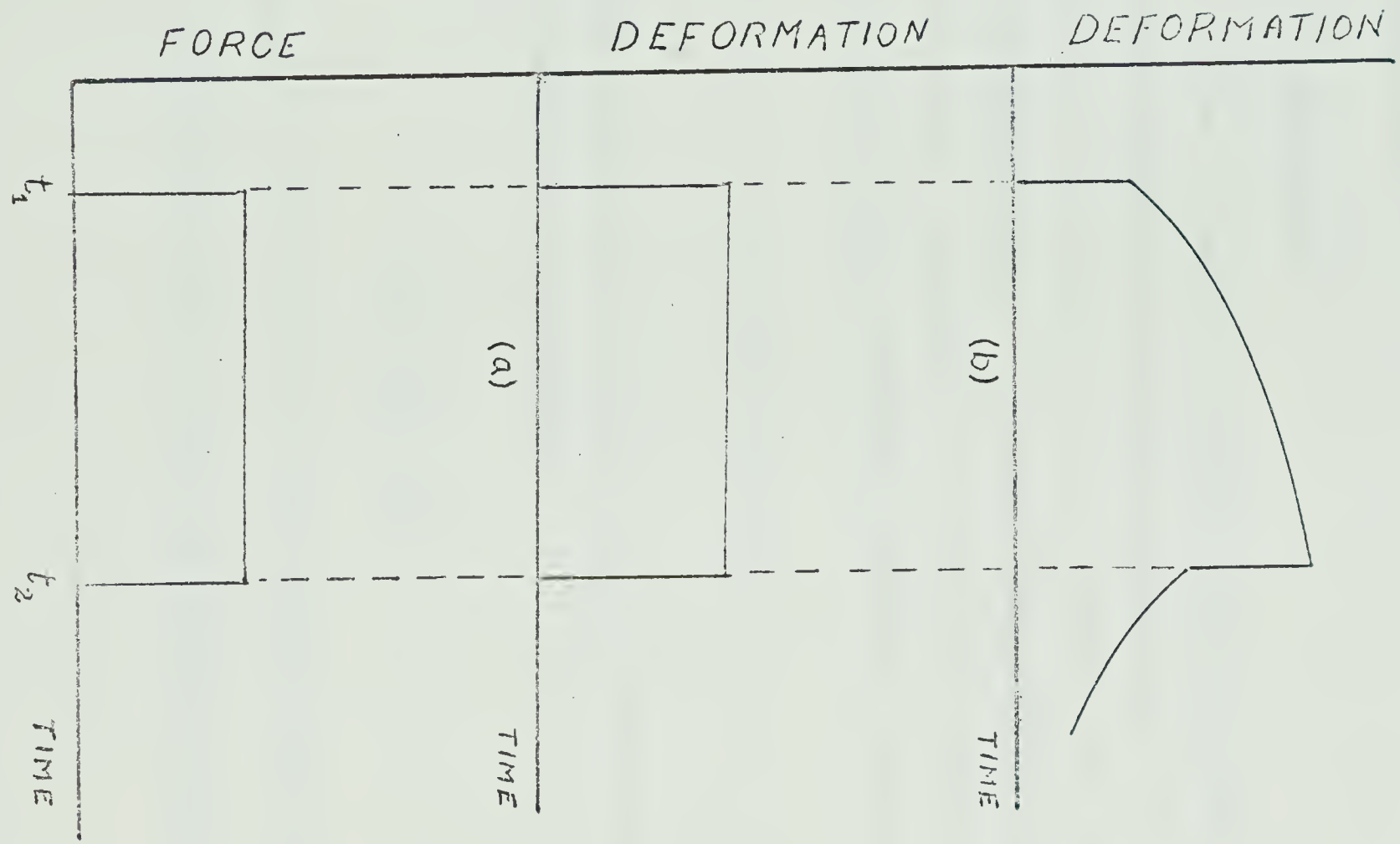
FORCE
DEFORMATION
DEFORMATION
t_1
t_2
TIME
(a)
TIME
(b)
TIME

taken in Hooke's law. Even while still within the elastic limit, a real solid does not behave elastically but rather in the manner depicted in figure 2.2(b).

(2) Anelasticity

In order to describe the behavior within the elastic limit, one must modify equation (2.2) so that it includes terms in the various orders of the time derivitive of the stress and strain components (Poynting and Thomson, 1905). A very good approximation to this is given by the equation containing only the first time derivitives of stress and strain. The one dimensional equation for this case is written:

$$a_1\sigma + a_2\dot{\sigma} = b_1\epsilon + b_2\dot{\epsilon} \quad . \tag{2.4}$$

This equation contains three independent constants which are chosen such that the equation can be written,

$$\sigma + \tau_\epsilon\dot{\sigma} = M_R(\epsilon + \tau_\sigma\dot{\epsilon}). \tag{2.5}$$

Solids which obey this equation are called standard linear solids.

We now suppose that a stress σ_o is suddenly applied at $t = 0$

and is held constant thereafter; then equation (2.5) becomes;

$$\sigma_o = M_R(\epsilon + \tau_\sigma \dot{\epsilon}) \; ; \quad t > 0,$$

which when rewritten is,

$$\epsilon + \epsilon\tau_\sigma^{-1} = (M_R \tau_\sigma)^{-1}\sigma_o \; .$$

The solution to this equation is,

$$\epsilon(t) = M_R^{-1}\sigma_o + (\epsilon_o - M_R^{-1}\sigma_o)e^{-t/\sigma} \; , \tag{2.6}$$

showing that the behavior of the standard linear solid is as that shown in figure 2.2(b) for a real solid. It is seen that the strain ϵ is equal to ϵ_o at a time t equal to zero and then relaxes to its maximum value $M_R^{-1}\sigma_o$ as t becomes large. Since, after all relaxation has occured,

$$\lim_{t \to \infty} \frac{\sigma}{\epsilon} = M_R \; , \tag{2.7}$$

the constant M_R will be called the relaxed modulus.

In order to find the physical significance of τ_ϵ and τ_σ we suppose a case where ϵ and $\dot{\epsilon}$ are identically zero. Then equation (2.5) reads,

$$\sigma + \tau_\epsilon \dot{\sigma} = 0,$$

whose solution is

$$\sigma(t) = \sigma(0)e^{-t/\tau_\epsilon}.$$

This indicates that τ_ϵ is the relaxation time of the stress under conditions of constant strain; similarly τ_σ is the relaxation time of the strain under constant stress.

Now if we consider a variation in stress $\Delta\sigma$ inducing a variation in strain $\Delta\epsilon$ over a vanishingly small time δt, we find from equation (2.5):

$$\Delta\sigma = M_R \frac{\tau_\sigma}{\tau_\epsilon} . \qquad (2.8)$$

The quantity $M_R\tau_\sigma/\tau_\epsilon$ will be note M_u and is called the unrelaxed modulus since it relates changes in stress and strain which occur in such a short period of time that no relaxation has time to occur.

Since the present investigation is concerned with the behavior of solids under periodic stress we must investigate the properties of

equation (2.5) with this in mind. In substituting into this equation the following solutions:

$$\sigma(t) = \sigma_o e^{i\omega t} \quad ; \qquad \text{and} \qquad \epsilon(t) = \epsilon_o e^{i\omega t} \ ,$$

it is found that

$$\sigma_o = \mathcal{M} \epsilon_o \ ,$$

where $\mathcal{M}$ is complex and given by,

$$\mathcal{M} = \frac{1 + i\omega\tilde{\tau}_\sigma}{1 + i\omega\tilde{\tau}_\epsilon} M_R \ . \tag{2.9}$$

The fact that the modulus relating σ and ϵ is complex indicates that the strain lags behind the stress by a phase which we shall denote δ. It is easily seen that

$$\tan \delta = \frac{\text{Im } \mathcal{M}}{\text{Re } \mathcal{M}} ,$$

which is evaluated from (2.9) to obtain:

$$\tan \delta = \frac{\omega(\tilde{\tau}_\sigma - \tilde{\tau}_\epsilon)}{1 + \omega^2(\tau_\sigma \tilde{\tau}_\epsilon)} \ , \tag{2.10}$$

If mechanical vibrations are set up in a specimen by a periodic stress;

$$\sigma = \sigma_o \cos \omega t,$$

the resulting strain will be, in general,

$$\epsilon = \epsilon_o \cos (\omega t - \delta).$$

The rate at which energy will be dissipated per unit volume during such vibrations is the mean value of σ , then the total power dissipation for a sample will be:

$$P = \int \overline{\sigma \dot{\epsilon}}\, dv,$$

$$P = \frac{\omega}{2} \sin \delta \int \sigma_o \epsilon_o dv, \qquad (2.11)$$

If tan δ is small then the vibrational energy per unit volume can be taken as $\frac{1}{2}\sigma_o\epsilon_o$ so that the total energy is

$$E = \frac{1}{2}\int \sigma_o \epsilon_o dv . \qquad (2.12)$$

A standard quantity Q^{-1} will now be defined in the usual way for a

driven oscillator:

$$Q^{-1} = \frac{\text{Power dissipation}}{\omega \times \text{energy of vibration}} ,$$

where ω is the angular frequency of the vibrations. For the case of the standard linear solid, it is seen from equation (2.11) and (2.12) that

$$Q^{-1} = \sin \delta , \tag{2.13}$$

and since tan δ was assumed to be small,

$$Q^{-1} \approx \tan \delta . \tag{2.14}$$

Tan δ has been evaluated in terms of the relaxation times in equation (2.10).

Equation (2.14) states that the normalized power dissipation in a standard linear solid is non zero since tan δ is non zero, that is vibrations are damped due to the fact that some of their energy is being dissipated to the medium. Since a real solid's behavior is approximated by the standard linear solid, vibrations should also be

damped in their case, and it is a well known experimental fact that this is true.

It has been seen that the value of Q^{-1} is a measure of the amount of damping that vibrations in a real solid are submitted to. Experimentally, Q^{-1} could be measured by measuring the phase lag of the induced periodic strain relative to the stress applied. This however is a difficult task since the angle δ is usually a very small quantity. In order to avoid this, Q^{-1} must be related to other quantities more easily measured in the laboratory.

However before discussing the measurement of Q^{-1} we shall return to equation (2.10), which can now be written:

$$Q^{-1} \approx \tan \delta = \frac{\omega(\tau_\sigma - \tau_\epsilon)}{1 + \omega^2(\tau_\sigma \tau_\epsilon)} , \qquad (2.15)$$

to see some of its other properties. We first define the geometric mean of the two relaxation times τ_ϵ and τ_σ as,

$$\overline{\tau} = (\tau_\epsilon \tau_\sigma)^{1/2} , \qquad (2.16)$$

and that of the two elastic moduli, M_u and M_R as,

$$\bar{M} = (M_u M_R)^{1/2} . \tag{2.17}$$

Using these definitions, equation (2.15) may be rewritten as,

$$Q^{-1}_{(\omega)} = \frac{M_u - M_R}{\bar{M}} \frac{\omega\bar{\tau}}{1+(\omega\bar{\tau})^2} , \tag{2.18}$$

which gives the frequency dependence of Q^{-1}. Equation (2.18) is depicted in figure 2.3. The maximum value of Q^{-1} which occurs at $\omega\bar{\tau} = 1$, is given by:

$$Q^{-1}_{max} = \frac{M_u - M_R}{2\bar{M}} .$$

It was shown in equation (2.9), for the case of periodic stress the elastic modulus is complex. It is of value to define a real modulus M which can be measured experimentally. We choose to define it as,

$$M_\omega = \left[\mathrm{Re}\ \mathcal{M}^{-1}\right]^{-1} ,$$

that is M_ω is the ratio of the stress to that part of the strain which

Figure 2.3

The frequency dependence of Q^{-1} and M_ω (after Zener, 1948)

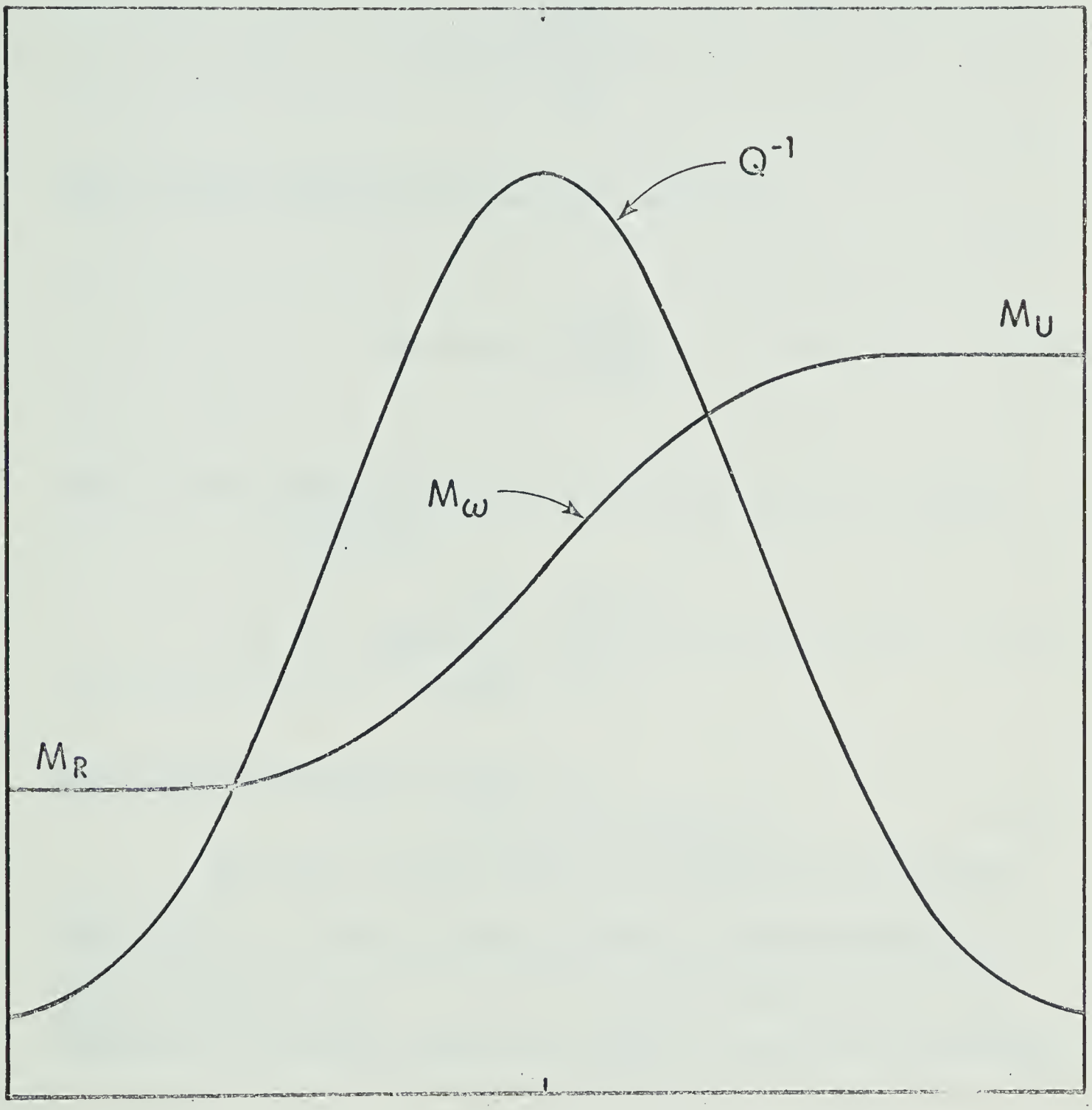
Q^{-1}
M_U
M_ω
M_R
$\omega\bar{\tau} = 1$
LOG $\omega\bar{\tau}$

is in phase with it (Zener, 1948, pp.47). From equation (2.9) it is seen that

$$M_\omega = \frac{1+\omega^2\tau_\sigma^2}{1+\omega^2\tau_\sigma\tau_\epsilon} M_R \ .$$

Then by using equation (2.8) the final result is:

$$M_\omega = M_u - \frac{M_u - M_R}{1+(\omega\bar{\tau})^2} \ ,$$

which has the limiting values,

$$M_\omega = \begin{cases} M_R \ ; & \omega\bar{\tau} \ll 1 \\ M_u \ ; & \omega\bar{\tau} \gg 1 \end{cases} \ .$$

This behavior is shown in figure 2.3.

The theory presented above was developed for the standard linear solid. It covers damping of vibrations characterized by a single relaxation time $\bar{\tau}$. It is a very good approximation to the behavior of red solids in which the damping is governed by one relaxa-

tion time. It is possible as well to develop a theory which covers damping with a spectrum of relaxation times by superposition of the results of each relaxation time in the spectrum. This, however, does not give a great deal of insight into the physical phenomena involved and for this reason most data is today analysed from first principles rather than the relaxation spectrum of a phenomenological theory. For example, in the theoretical interpretation of damping due to electron phonon interaction, one considers the rate of energy dissipation due to the disturbance of the viscous electron gas by the vibration phonons (Bhatia, 1967).

(3) Definition of Parameters Related to Elastic Energy Dissipation

It is now necessary to return to the parameter Q^{-1}. From the defining equation it is known that:

$$Q^{-1} = \frac{\text{Power dissipation}}{\omega \times \text{energy of vibration}} . \qquad (2.19)$$

If we define ΔE as the energy dissipated per cycle of vibration of total energy E, then,

$$\frac{\Delta E}{E} = \frac{2\pi \text{ Power dissipation}}{\omega E} . \qquad (2.20)$$

On comparing equations (2.19) and (2.20) it is found that,

$$Q^{-1} = \frac{1}{\pi} \left(\frac{1}{2} \frac{\Delta E}{E}\right) , \qquad (2.21)$$

thus Q^{-1} has been related to the energy dissipated during one half cycle of vibration. The energy E must now be related to the amplitude of vibration which is a measurable quantity. Since elastic energy is dissipated, the amplitude of free vibrations must decrease in time. Suppose the amplitude at the beginning and the end of a period of time, equal to the period of the vibration, is known. These amplitudes will be noted A and $A-\Delta A$ respectively. A new parameter called the logarithmic decrement is now defined as,

$$\text{logarithmic decrement} = \ln \frac{A}{A-\Delta A} . \qquad (2.22)$$

Since the elastic energy of the vibration is proportional to the square then,

$$\ln \frac{A}{A-\Delta A} = \ln \frac{E^{1/2}}{(E-\Delta E)^{1/2}} , \qquad (2.23)$$

where ΔE was defined for equation (2.21). If ΔE is small it is easily shown that,

$$\text{log. dec.} = \ln \frac{A}{A-\Delta A} = \frac{1}{2} \frac{\Delta E}{E} , \qquad (2.24)$$

In comparing equations (2.21) and (2.24) it is seen that :

$$\text{log. dec} = \pi Q^{-1}. \qquad (2.25)$$

From equation (2.15) it is seen that Q^{-1} is dependent on frequency and the two relaxation times τ_σ and τ_ϵ. Since the frequency is independent of amplitude and it is assumed that the relaxation times are also independent of amplitude then equation (2.25) can be written in the form;

$$A(t) = A(0) \exp.(-\frac{Q^{-1}}{2})\omega t . \qquad (2.26)$$

This shows that in a standard linear solid the amplitude of free vibrations decays exponentially. It is a well established experimental fact that in real solids for the most part the decay of vibrations is exponential. This suggests a method for measuring Q^{-1}; that is by measuring A(t) for free decay and evaluating the exponential. This method is practical for valuo of the dissipation which give decay times that

are long enough to be measured accurately.

Suppose we have a sample which is in forced vibration near its resonant frequency. It is possible, in this case, to evaluate the dissipation from the shape and frequency of the resonance peak. It is assumed that the sample can be represented by a system with one degree of freedom and with an anelastic restoring force, f, similar to the standard linear solid. If the displacement from equilibrium of this system is noted x, then the equation of motion can be written,

$$\rho\ddot{x} + f = F_o e^{i\omega t} ,$$

where ρ is the inertia of our system and F_o the amplitude of the driving force. The restoring force is related to the displacement by:

$$f = \mathcal{M} x = M(1 + i \tan \delta)x ,$$

where $\mathcal{M}$ is the complex elastic modulus. Assuming a solution of the form:

$$x = x_o e^{i\omega t} ,$$

and substituting into the equation of motion, it is seen that,

$$x_o = \frac{F_o/M}{(1 - \frac{\rho v^2}{M}) + i \tan \delta} \quad . \qquad (2.27)$$

The amplitude of the displacement is seen to have a maximum at the frequency ω_o given by:

$$\omega_o = (\frac{M}{\rho})^{1/2} \quad ,$$

and to have half this maximum value when

$$1 - \frac{\omega^2}{\omega_o^2} = \pm \sqrt{3} \tan \delta \quad .$$

From equation (2.14) it is known that

$$Q^{-1} = \tan \delta \quad ,$$

therefore, Q^{-1} is related to the width of the resonance peak at half maximum, denoted by $\Delta\omega$, in the following way:

$$Q^{-1} = \frac{\Delta\omega}{\sqrt{3}\,\omega_o} \quad . \qquad (2.28)$$

CHAPTER III

EXPERIMENTAL TECHNIQUE

A. Samples and Mounting

The material to be investigated in this work was polycrystaline iron, more specifically Johnson, Matthey spectrographically standardized iron. It was purchased in the form of a plate of 3 mm thickness from which disks were cut with diameters of 30 and 36 mm. The resonance technique was used to investigate the acoustic damping in this material; that is the samples were excited to vibration in their flexural normal modes and depending on circumstances (either the rate of decay of free vibration or the width of the resonance peak was measured. The method of mounting the samples in the cryostat was that described by Bordoni, Nuovo, and Verdini (1959).

The point behind this method is minimizing any damping of vibrations in the specimen due to the surroundings. One cause of external damping is acoustic radiation from the sample to the surrounding air. This is effectively nullified by placing the sample in an evacuated chamber. All the measurements presented here were done at pres-

sures of less than 10^{-4} mm Hg. The next problem arises with supporting the sample in the chamber. A schematic diagram of the mount used is shown in figure 2.1. It consists of resting the sample on three sharp pins which come into contact with it on a nodal circle and are separated by 120° on that circle. In order to prevent the sample from moving on the pins, three shallow holes were drilled at the points of contact of the pins. The fact that the sample was contacted only at three sharp points located on a nodal circle minimized the amount of elastic energy transferred from the sample to its mount.

These pins served other functions, as well as being a low damping support. One pin was steel and provided a ground connection for the sample to the cryostat as illustrated by "3" in figures 3.1 and 3.2. The other two pins (1 and 2 in figures 3.1 and 3.2) were in the form of fine wires of about 0.33 mm in diameter, insulated from ground and were used as a thermocouple with the sample forming the junction. The material used for the thermocouple was gold + 2.1 At % Co referenced to copper. This was chosen because it is the most sensitive low temperature thermocouple readily available (Powell et al., 1961).

B. The Excitation and Detection of Vibrations

The vibrations in the sample were excited by an electrostatic

Figure 3.1

Schematic diagram of the sample mount.

C - nodal circle

E - driving electrode

P - support pins

1 and 2 - thermocouple

3 - ground pin

S - sample

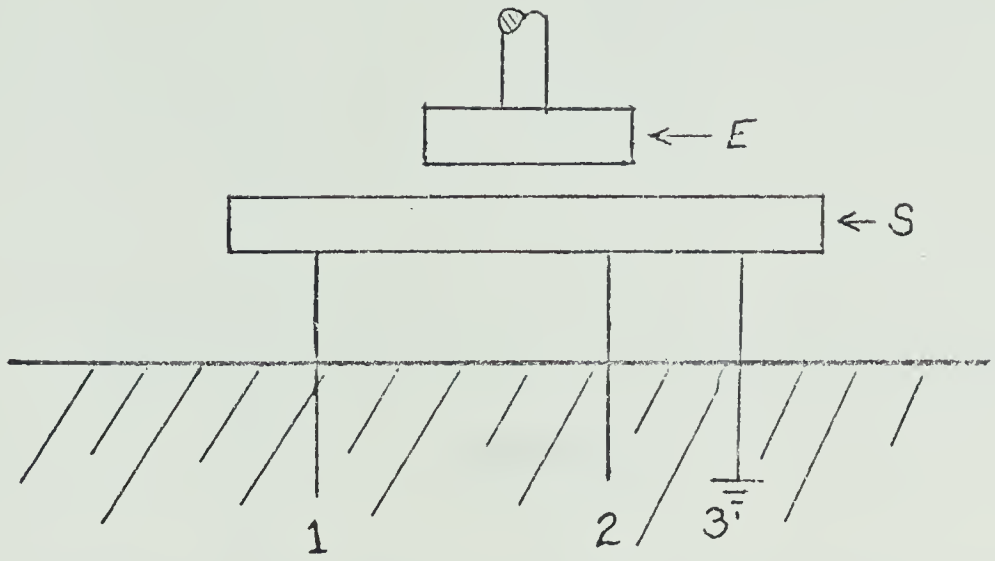
E
S
1
2
3

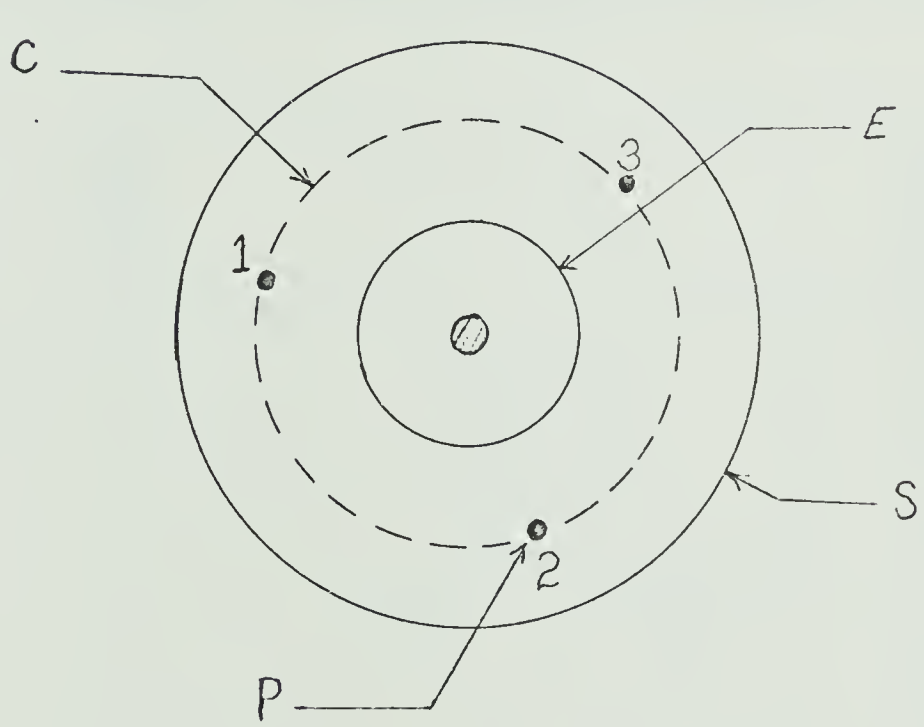
C
E
3
1
S
2
P

Figure 3.2

Schematic diagram of the Cryostat showing the sample mounted (see figure 3.1 for labels)

A, B and C - level adjustments for support pins

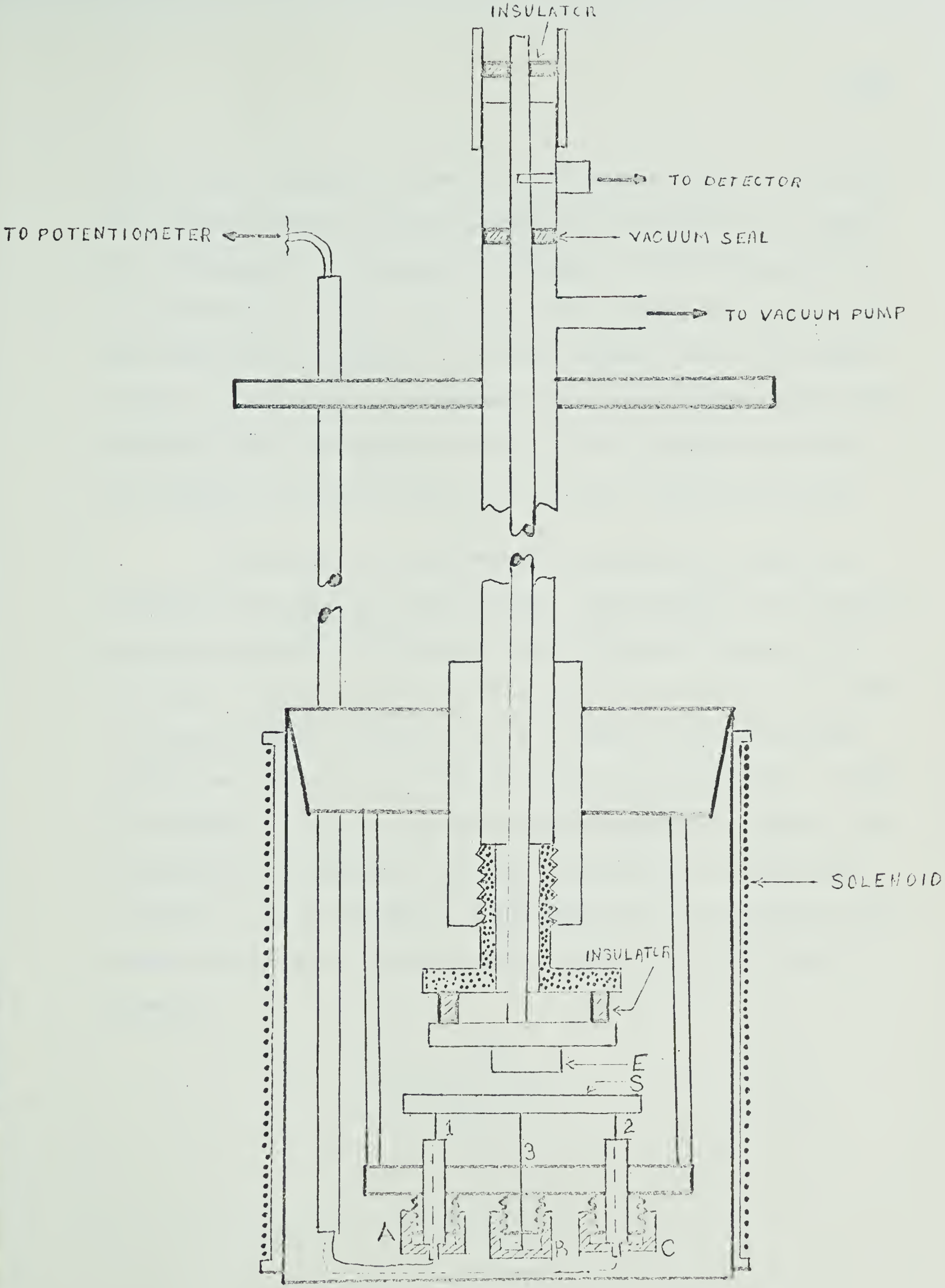
INSULATOR
TO DETECTOR
TO POTENTIOMETER
VACUUM SEAL
TO VACUUM PUMP
SOLENOID
INSULATOR
E
S
1
2
3
A
B
C

force from an electrode, in the form of a plate of about 6 mm in diameter, placed directly above and parallel to the surface of the sample at a distance of a few tenths of a millimeter. This is illustrated by E in figure 3.1 and 3.2. The distance of the electrode from the sample was controlled by turning it in a finely threaded mount in the sample chamber. The turning was accomplished via a small diameter, thin wall, stainless steel tube connected directly to the electrode and exiting the cryostat up the main pumping line through a rubber vacuum seal.

The control rod was insulated from ground and served as an electrical feed-through to the electrode. The excitation and detection circuits connected to this rod are shown in the block diagram of figure 3.3. In order to excite the vibrations in the sample, it was kept at ground potential by means of pin 3 in figure 3.2 and a sinosoidal voltage was applied to the electrode through the control rod. In order to calculate the force on the sample due to a voltage V applied to the electrode it is necessary to consider the system as a parallel plate capacitor. If the capacitance of the system is C and the charge on the plates is given by q, then the energy W stored in the system will be given by:

$$W = \frac{1}{C} \int_0^q q' dq' \ ,$$

Figure 3.3

Block diagram of the experimental set up

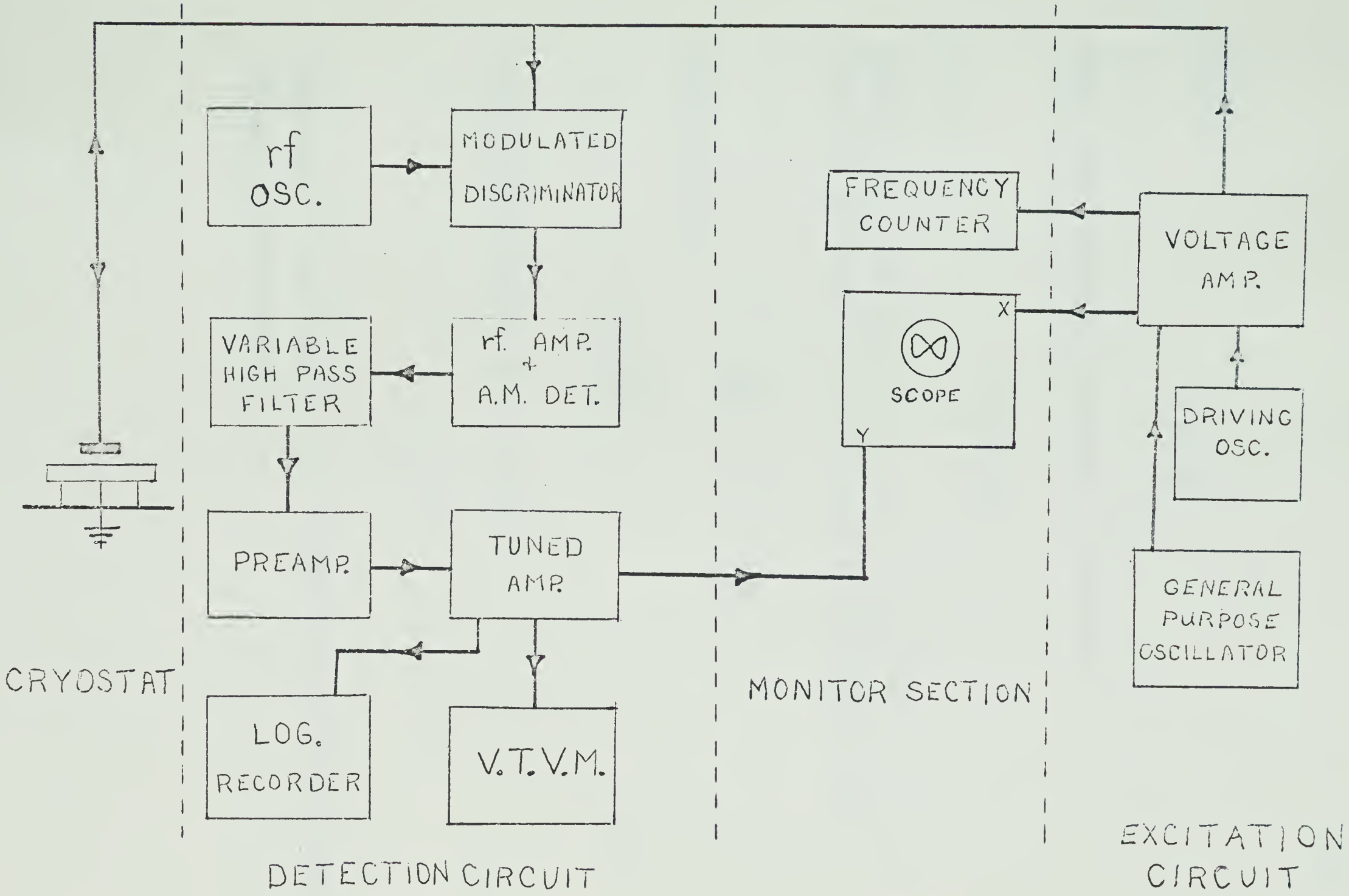
rf
OSC.
MODULATED
DISCRIMINATOR
VARIABLE
HIGH PASS
FILTER
rf. AMP.
+
A.M. DET.
PREAMP.
TUNED
AMP.
LOG.
RECORDER
V.T.V.M.
CRYOSTAT
DETECTION CIRCUIT
FREQUENCY
COUNTER
X
SCOPE
Y
VOLTAGE
AMP.
DRIVING
OSC.
GENERAL
PURPOSE
OSCILLATOR
MONITOR SECTION
EXCITATION
CIRCUIT

therefore,

$$W = \frac{1}{2} \frac{q^2}{C} .$$

Since, for a parallel plate capacitor, C is given by:

$$C = \epsilon_o \frac{A}{d} ,$$

where ϵ_o is the permittivity, A the area of the plates and d the distance that separates them, then the force F on the sample, using:

$$F = - \frac{\partial W}{\partial d} , \quad \text{and} \quad C = \frac{q}{V} ,$$

will be given by:

$$F = \frac{\epsilon_o A}{2d^2} V^2 . \qquad (3.1)$$

If the applied voltage V is of the form:

$$V = V_o e^{i\omega t} ,$$

then, since the resulting force F is proportional to the square of this voltage, it will be given by:

$$F = F_o e^{2i\omega t},$$

which is an oscillating force of frequency 2ω. This force will then set up flexural vibration in the sample of this same frequency 2ω.

The driving voltage came from an oscillator-amplifier combination whose output level could be varied from 0 to 250 volts over a frequency range of 2 KH_z to 300 KH_z. The voltage amplifier was built in this laboratory and was similar to that described by Nuovo (1961). The oscillator was constructed to have a wide band and high stability according to the circuit shown in figure 3.4. The tuning was such to allow a change of the output frequency by less than 0.1 H_z over the entire frequency range. The frequency stability was found to be better than 0.1 H_z after a few hours of operation. The fine tuning ability was achieved by using a 100 to 1 mechanical reduction on the controls of the variable capacitors A and B. In summary, the vibrational state of the sample was controlled by the frequency and amplitude of the driving voltage and the distance of the electrode from the specimen.

The fact that the electrode and the sample formed a parallel plate capacitor was taken advantage of in order to measure the amplitude of the excited vibrations. When the sample was vibrating its average

Figure 3.4

Cathode-coupled oscillator used for the driving voltage

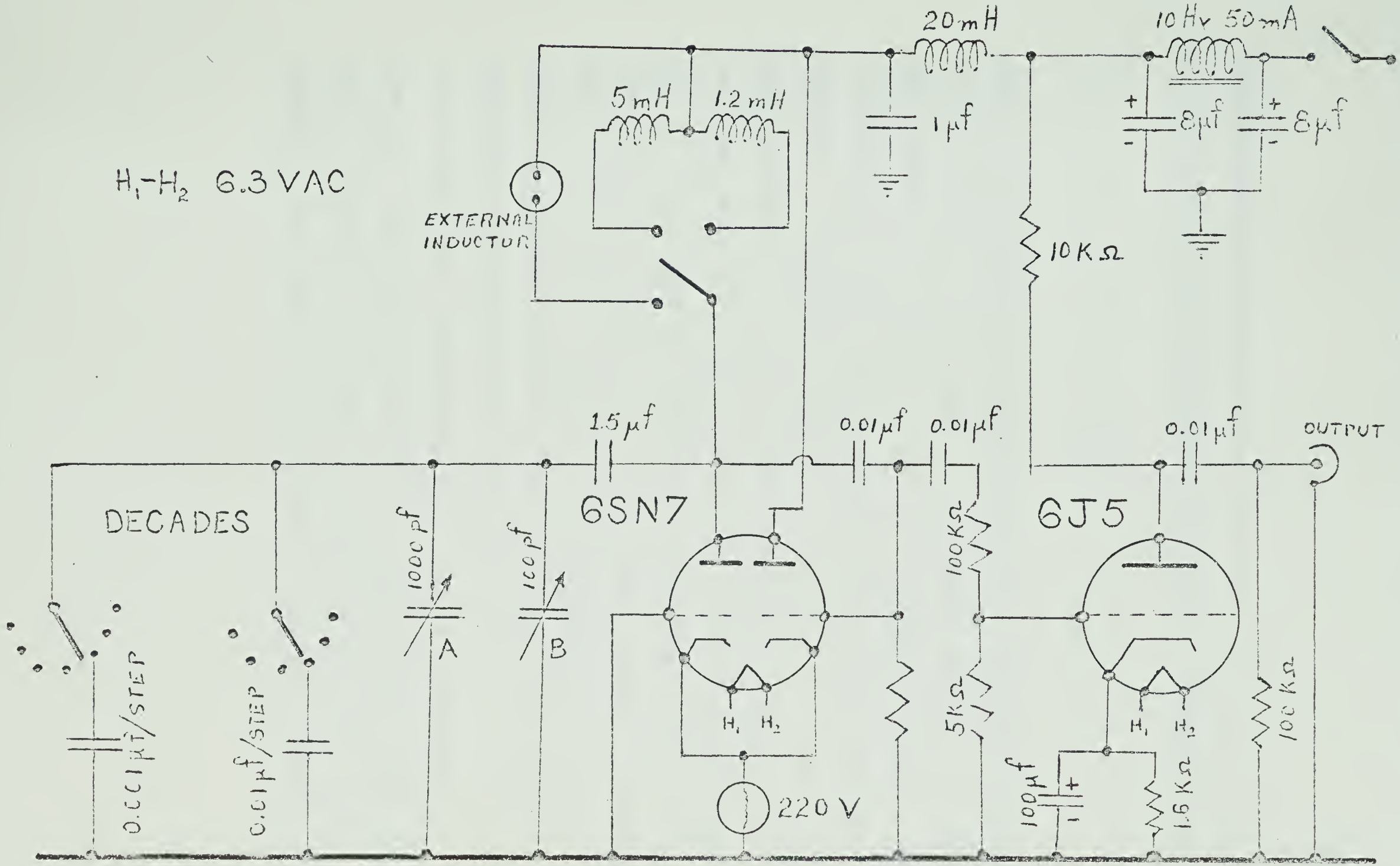
H_1-H_2 6.3 VAC
EXTERNAL INDUCTOR
5 mH
1.2 mH
20 mH
1 μf
10 Hy 50 mA
8 μf
8 μf
10 KΩ
1.5 μf
0.01 μf
0.01 μf
0.01 μf
OUTPUT
6SN7
6J5
DECADES
0.0001 μf/STEP
0.01 μf/STEP
100 pf
100 pf
A
B
100 KΩ
5 KΩ
100 μf
1.6 KΩ
100 KΩ
H_1 H_2
H_1 H_2
220 V

distance from the electrode varied in a sinosoidal way thereby causing a variation, C, in the capacitance of the system. Considering that:

$$C \alpha \frac{1}{d},$$

where d is the electrode to sample distance then a sinosoidal variation in d of amplitude Δd will produce a corresponding variation in C whose amplitude will be proportional to Δd. The experimental problem is now to measure ΔC in order to get a relative measure of the vibrational amplitude. In referring to chapter II, section B(3) it is seen that a measure of relative amplitude suffices to specify the magnitude of Q^{-1}. The measurement of ΔC is done by including the sample-electrode capacitor, C, in an antiresonant discriminator circuit whose input is connected to an rf. oscillator with a 10 MH_z output. Because of the variation in C the "resonant" frequency of the discriminator is modulated causing an amplitude modulation of the 10 MH_z signal across the discriminator. The frequency of the side bands is the same as that of ΔC and their amplitude is proportional to it, thus to the amplitude of vibration. This circuit was described in a paper by Nuovo (1961) along with the demodulator which produced an audio frequency signal corresponding to the sidebands of the modulated rf. signal, and therefore

the vibration of the specimen.

This signal was then put through a variable high-pass filter, set at about 5 KH_z below the frequency of vibration, to cut out low frequency noise such as room vibrations and any leak-through which might have occurred from the driving signal. The signal was then routed through a tuned amplifier system whose circuit is illustrated in figure 3.5. The tuned stage of this amplifier has a Q which is much lower than the mechanical one in order to avoid interference with the measurements. The amplified signal was then fed into a logarithmic level recorder (Bruel and Kjaer, Model 2305) and vacuum tube volt meter. This signal was also used as the y input of an oscilloscope whose x input was connected to the driving signal. The 2 to 1 Lissajou figure displayed served as a monitor for the detected and driving signals. The driving signal frequency was measured to an accuracy of $\pm$ 0.1 H_z by a frequency counter connected to the output of the voltage amplifier.

C. Temperature Measurement

After the frequency and relative amplitude of the vibrations are known, a third parameter is needed, namely the temperature of the specimen. The thermocouple described earlier provides this information. The reference junction was placed in an ice bath whose temperature was

Figure 3.5

Preamplifier and tuned-amplifier used in the detection circuit

DECADE CAPACITORS
A – 0.01 μf/STEP
B – 0.001 μf/STEP

H_1-H_2 6.3 VAC

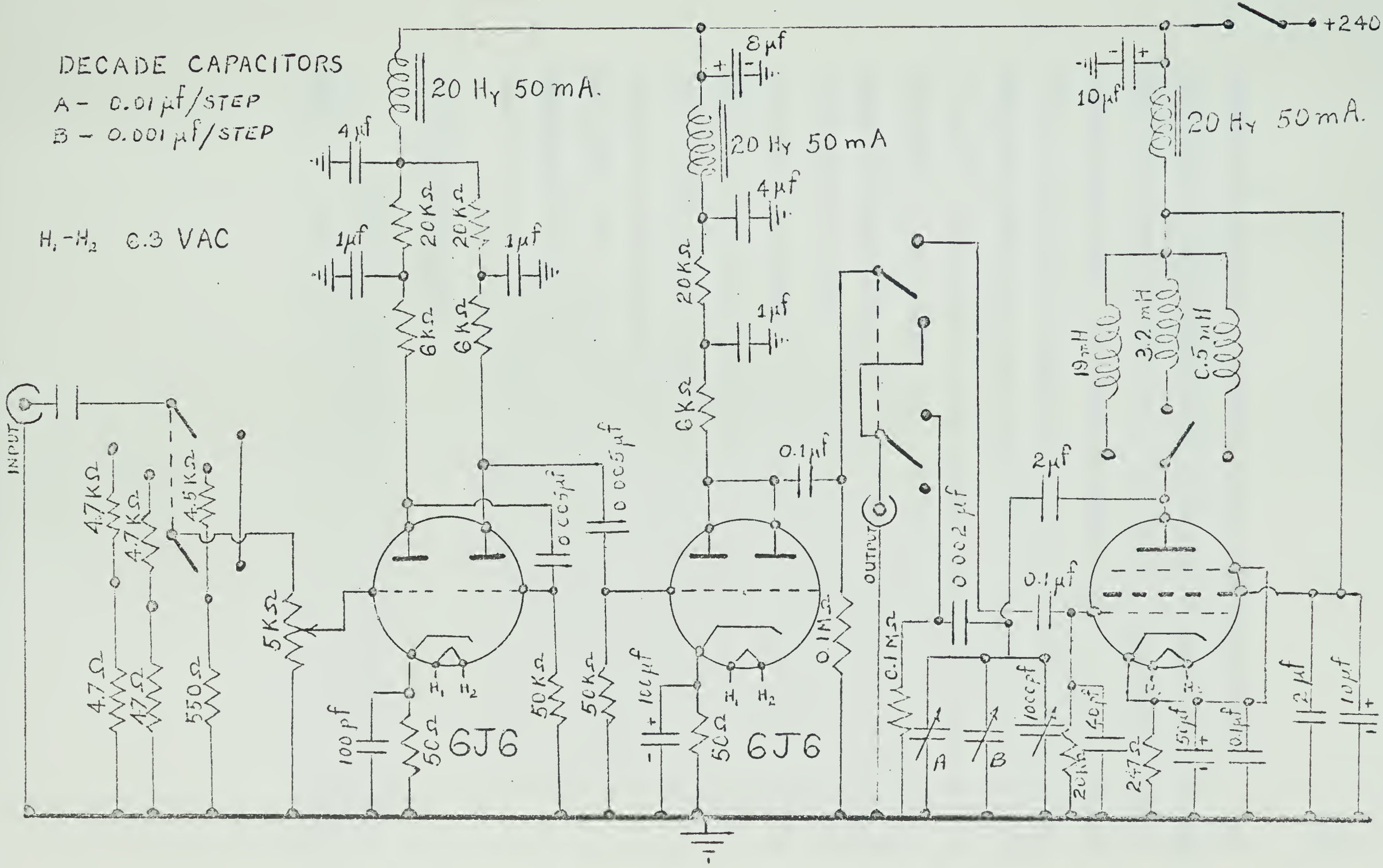

monitored by a mercury thermometer with a resolution of 0.1° C. The calibration of this thermoccuple was derived from data given by Powell, Bunch, and Corruchini (1961) for a gold plus 2.1 At. % cobalt versus copper thermocouple. To do this the thermocouple e.m.f. was measured at the boiling point of oxygen and helium and the ratio between these values and those given by the above authors were compared and found to be equal to within 0.1% so it was assumed that it would be a constant throughout the temperature range. From this assumption a table was prepared giving thermocouple e.m.f. versus temperature at intervals of 0.5° K from 1 to 300° K. The output of the thermocouple was measured by standard potentiometric means and compared to this table by interpolation to arrive at the temperature of the sample. Since the whole of the sample formed the junction of the thermocouple, the temperature measured in this way was the average temperature of the sample. The precision of this measurement was estimated to be ± 0.2° K from room temperature to about 15° K. Below this temperature, the error increased to its maximum value of ± 0.5° K at helium temperatures.

D. Operating Procedure

In order to demonstrate the use of the equipment described above it is instructive to go through the operations of a typical data

run. The first step is to set the sample on the support pins and to adjust the pin holders (A,B and C in figure 3.2) so that the sample is parallel to the electrode. If the sample were not parallel to the electrode the sensitivity of the detector circuit would be markedly reduced. The can is then put into place and the chamber evacuated. The sample is now ready for the measurements. The resonant frequency is found by connecting the input of the driving voltage amplifier to a general purpose wide band oscillator and sweeping the frequency through the region where it is expected. A table giving the characteristics of the first flexural vibration modes in a thin circular plate is given in Appendix I. The driving oscillator is now tuned to this frequency and switched into the amplifier. The filter is then switched into the detection circuit and the tuned amplifier is adjusted for maximum gain. The sample is now being driven at one of its resonant frequencies and these vibrations are being detected and displayed on the oscilloscope along with the driving voltage.

A quick check at this point will indicate whether the width of the resonance peak is sufficient to allow measurement, or not. Since the frequency counter will only allow measurements of this width to within 0.2 H_z it is necessary that it be several H_z in order to get an accurate value for Q^{-1}. If it is possible to make this measurement

then by using the vacuum tube voltmeter and frequency counter the two frequencies f_1 and f_2 at which the amplitude of vibration is one half that at resonance are measured and Q^{-1} is calculated from,

$$Q^{-1} = \frac{f_2 - f_1}{\sqrt{3}\ f_o} \quad ,$$

which was given in Chapter II. A typical resonance curve is shown in figure 3.6(a).

When the resonance peak is too narrow to be measured with any appreciable accuracy, which occurs when the damping is low, another method must be used. A satisfactory method is to shut off the driving voltage and measure the rate of decay of the amplitude of vibrations at resonance. This is done by recording the detected signal on the logarithmic level recorder as a function of time. The trace of a typical decay is shown in figure 3.6(b). Since the decay of vibrations is exponential it produces a straight line on the recorder. This line is then extrapolated to 50 db and the time of this 50 db decay, t_{50}, is then determined from the recorder speed. The value of Q^{-1} can be calculated from this information using:

Figure 3.6

(a) Resonance curve for a specimen showing characteristic frequencies

(b) Typical logarithmic recording of the decay of vibrations

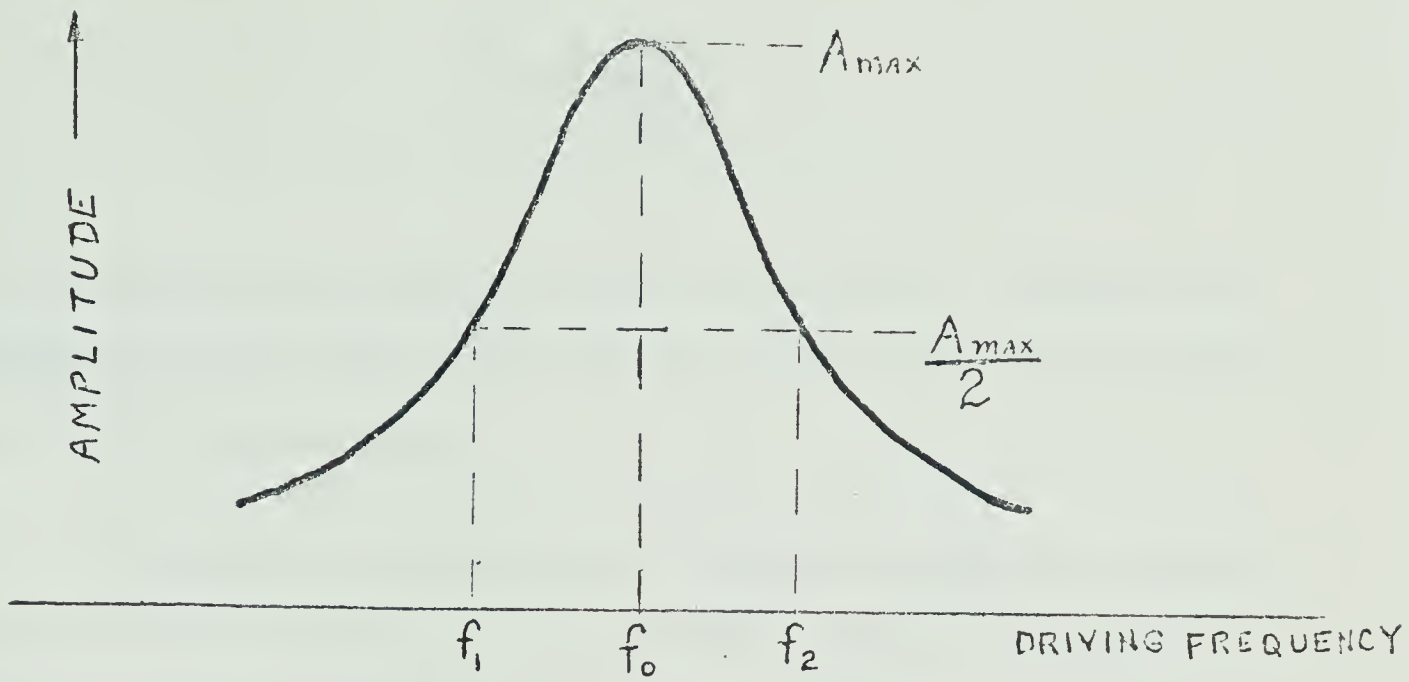
AMPLITUDE
A_{MAX}
$\frac{A_{max}}{2}$
f_1
f_o
f_2
DRIVING FREQUENCY

(a)

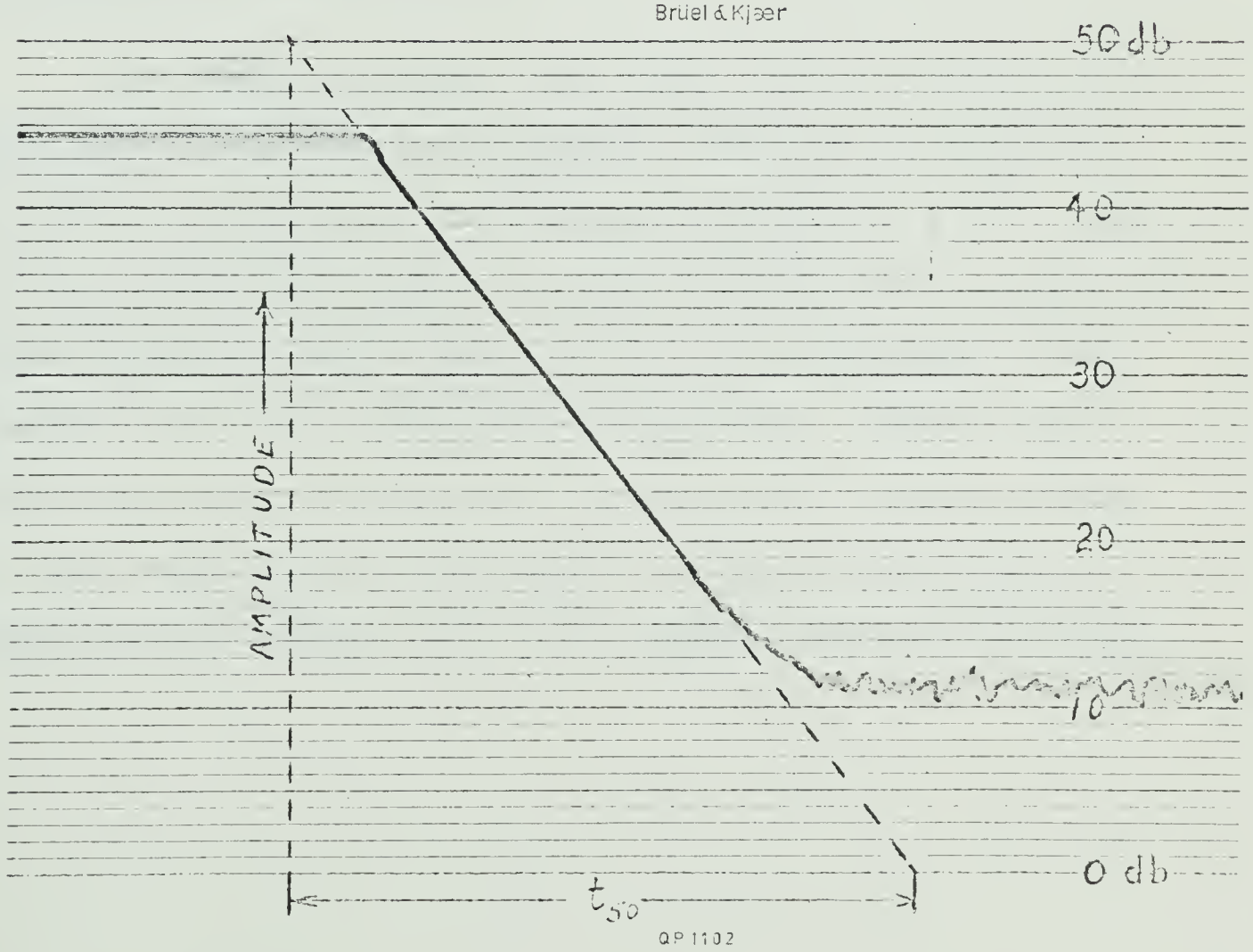
Brüel & Kjær
50 db
40
30
20
10
0 db
AMPLITUDE
t_{50}
QP 1102

(b)

$$Q^{-1} = \frac{1.833}{f_o \cdot t_{50}},$$

which was derived from equation (2.26) in chapter II. Satisfactory agreement has been found between the two methods when it was possible to use both at the same time.

It should be emphasized that these two methods are complementary. When the damping of the vibrations is high, the resonance peak is sufficiently wide to yield an accurate value of Q^{-1}. As the damping gets smaller, the peak becomes too narrow for measurement, however the decay time becomes long enough for accurate measurement, that is greater than 0.5 seconds.

The sample and chamber were cooled from room temperature to liquid helium temperature and measurements were made at intervals of 5° to 10° K in order to get the temperature dependence of Q^{-1}. The cooling was achieved by placing the chamber above a boiling liquid gas. Liquid nitrogen was used to cool to 77° K and the remainder of the temperature range was covered using liquid helium. Thermal contact between the sample and the chamber was maintained by helium exchange gas. The temperature was kept constant during the measurements by pumping out this exchange gas. At the beginning and end of each meas-

urement, the temperature was noted and it was found that the drift was within 0.2° K except when approaching the boiling point of liquid helium.

E. Cryostat Test

In order to estimate the damping of vibrations due to the background, that is the mount and the atmosphere around the sample, a trial run was carried out on a well annealed sample of tantalum. This metal was chosen because of its very low intrinsic damping as was shown by Bordoni (1961). The results of these measurements are shown in figure 3.7. As expected the damping decreases with temperature and, at about 15° K, Q^{-1} reaches a value of 2.66×10^{-7}. The damping measured below this temperature showed considerable amplitude dependence, which was attributed to damping due to external causes. It was estimated that external contribution to damping made up 30% of the recorded value, that is it was equivalent to a Q^{-1} of approximately 1×10^{-7}. This is less than 1% of damping measured in iron at its minimum value (refer chapter IV) so it shall be neglected in discussing the results.

Figure 3.7

The dependence of the dissipation coefficient, Q^{-1}, on temperature in tantalum (annealed in vacuum for 8 hrs. at 800° C)

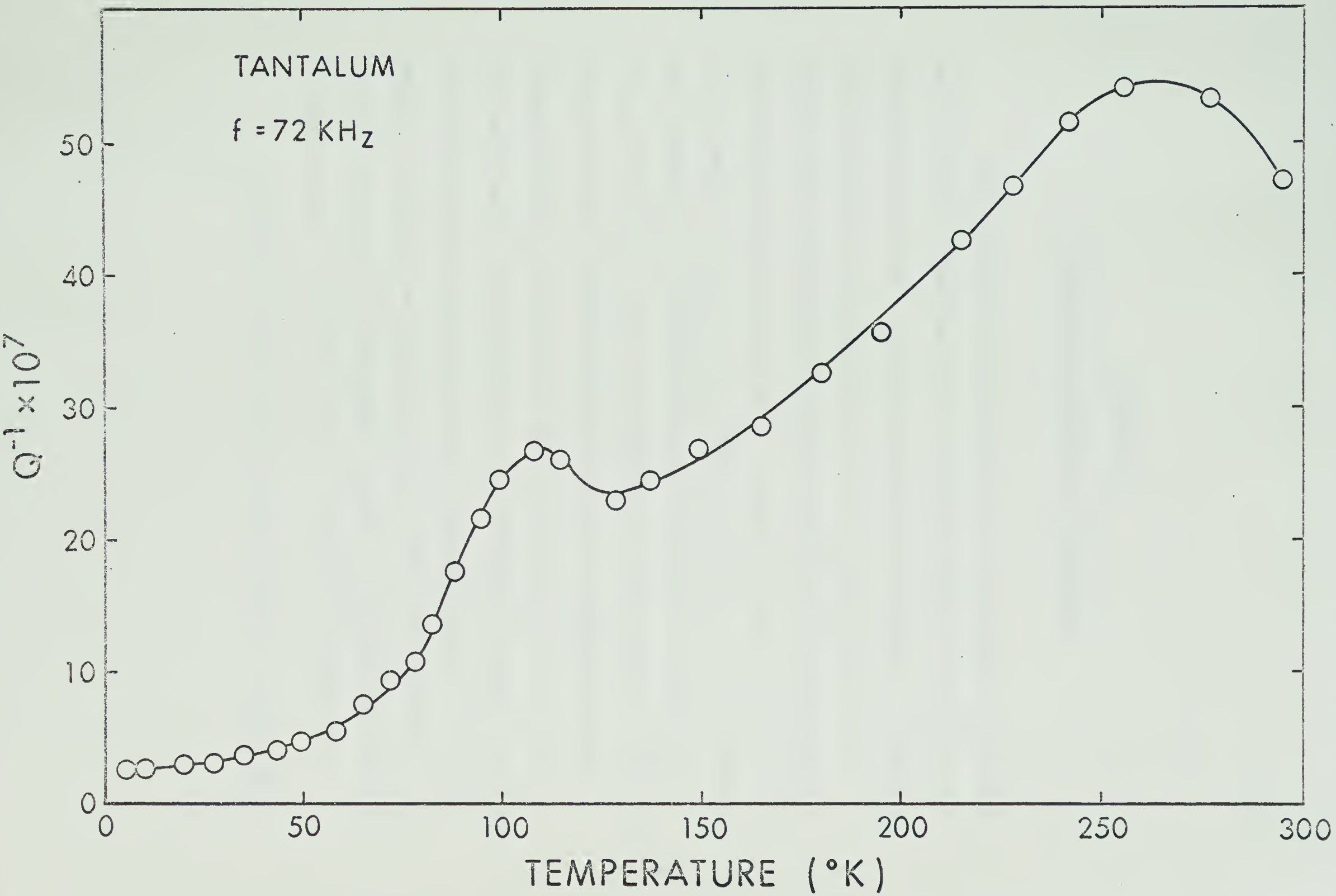
TANTALUM
f = 72 KHz
$Q^{-1} \times 10^7$
0
10
20
30
40
50
0
50
100
150
200
250
300
TEMPERATURE (°K)

CHAPTER IV

EXPERIMENTAL RESULTS AND DISCUSSION

The motivation for this work, as it was pointed out earlier, was to study the anomalous rise in vibration damping observed, at low temperature, in iron. Normally, in a metal, the damping of vibrations slowly decreases with temperature having its lowest value at 0° K (Mason, 1961). The first step in this study of iron was to measure the temperature dependence of Q^{-1}. The graph of figure 4.1 is a plot of the results obtained for four different frequencies. These frequencies represent the fundamental mode f_1 and the first harmonic f_2 of flexural vibrations without nodal diameters in two samples. These two samples were cut from the same plate and after machining they were annealed together in vacuum for eight hours at 400° C. At the end of this eight hours, the temperature of the samples was slowly reduced to room temperature by cycling it around a decreasing mean value. This method of annealing was found to give the lowest room temperature damping and the largest low temperature anomally. The physical dimensions of all the samples studied in the work are given in Appendix II.

In order to explain this anomalous behavior, its dependence

Figure 4.1

Dependence of Q^{-1}, in spectrographically pure iron, on temperature for several frequencies

Sample # 1
△: $f_1 \approx$ 28 KHz
○: $f_2 \approx$ 104 KHz

Sample # 2
□: $f_1 \approx$ 40 KHz
○: $f_2 \approx$ 140 KHz

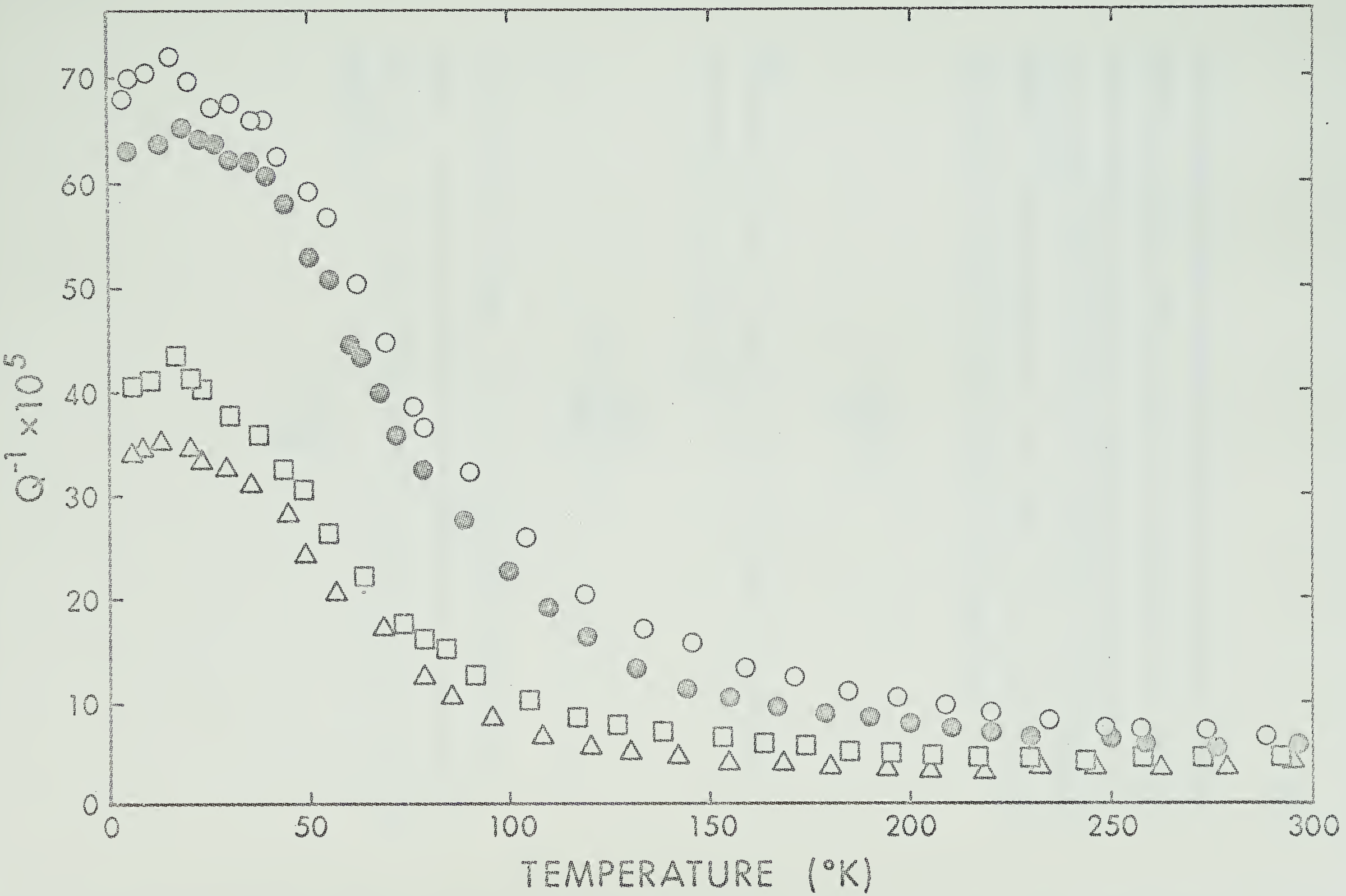
70
60
50
40
30
20
10
0
0
50
100
150
200
250
300
TEMPERATURE (°K)

on the amplitude of the vibrations must also be determined. The dissipation coefficient, Q^{-1} was found to be independent of the amplitude of the vibrations throughout the temperature and frequency range for all amplitudes used in this study. The calculation of this vibrational amplitude range was described by Nuovo (1961). It was shown in chapter III (equation 3.1) that the force applied to the sample was:

$$F = \frac{\epsilon_o A}{2d^2} V^2 .$$

Taking the real part of equation (2.27) we find that the amplitude of the vibrations X_o, is given by:

$$X_o = \frac{\epsilon_o A V_o^2}{2d^2 \rho \omega_o^2} \quad Q \quad ,$$

at the resonance condition. In order to apply this equation to the sample, A is taken as the area of the electrode and ρ as the density of the sample. The strain amplitude ϵ at the center of the plate will then be given by:

$$\epsilon = \frac{h}{2} \frac{X}{a_1^2} \quad ,$$

where h is the thickness of the plate and a_1 is the radius of the smallest nodal circle (see Appendix I).

The values of the parameters involved were within the following ranges:

$$5 \times 10^{-3} \text{ cm} \leq d \leq 5 \times 10^{-2} \text{ cm},$$

$$30 \text{ volts} \leq V \leq 100 \text{ volts},$$

$$10 \text{ mm} \leq a_1 \leq 15 \text{ mm},$$

$$10^3 \leq Q \leq 10^5,$$

$$60 \text{ KH}_z \leq \omega_o \leq 400 \text{ KH}_z$$

and,

$$A = 100 \text{ mm}^2,$$

$$h = 3 \text{ mm},$$

$$\rho = 8 \text{g/cm}^3.$$

Taking these into account, it is found that the range of the experimental strain amplitude is approximately given by:

$$5 \times 10^{-12} \lesssim \epsilon \lesssim 5 \times 10^{-9}.$$

This gives a maximum value to X of the order of a few Ängstrom units.

It can be seen, then, that the vibration amplitudes being studied are of the same order of magnitude as the interatomic distances. Any attempt to use vibrations with larger amplitudes than that mentioned above caused the dissipation to increase and become amplitude dependent. This, as yet unexplained, behavior is thought to be unrelated to the effect being studied in iron since it occured at all temperatures, including room temperature where the anomaly is found to be negligible. Any interpretation of the anomalous behavior must therefore show the amplitude independence of the dissipation, at least for low amplitude vibrations.

It was shown in Chapter 1 that Q^{-1} is a measure of the energy dissipated by vibrations to their supporting medium and it was pointed out that this dissipation may occur through more than one process. For this reason it will be considered that the measured values of Q^{-1} can be written in the following form:

$$Q^{-1} = Q_b^{-1} + \Delta Q^{-1} ,$$

where Q_b^{-1} is the damping due to dissipation of energy through all processes except that which causes the anomalous rise as low temperature. This rise is noted ΔQ^{-1}. The value of Q_b^{-1} was chosen to be slowly

decreasing and linear in temperature. This is illustrated in figure 3.1 and was justified at the beginning of this chapter by what is found in a normal metal. An example of this behavior is shown in figure 3.4 which gives the variation of Q^{-1} with temperature in nickel. The value of ΔQ^{-1} can now be found by simple subtraction. The dependence of ΔQ^{-1} on frequency, as derived from figure 4.1, is shown in figure 4.2 for various temperatures.

In his paper, Heller (1961) attempted to explain ΔQ^{-1} in terms of the magnetic properties of iron, more specifically the magnetostrictive properties. It was his contention that this anomalous behavior was related the the ΔE effect described by Bozorth (1951, pp. 684). If this interpretation is to be valid, then ΔQ^{-1} should be dependent on magnetic field. More specifically, the damping due to magnetostrictively induced eddy currents should go to zero at saturation fields. The data illustrated in figure 4.3 show no appreciable dependence of the damping on magnetic field. It was also thought advisable to measure the damping in other ferromagnetic metals in order to compare their behavior with that of iron. The results for nickel are shown in figure 4.4. There is no indication from thesedata that nickel behaves anomalously like iron does.

Figure 4.2

The variation of the anomalous dissipation coefficient, ΔQ^{-1}, with frequency for several temperatures in iron.

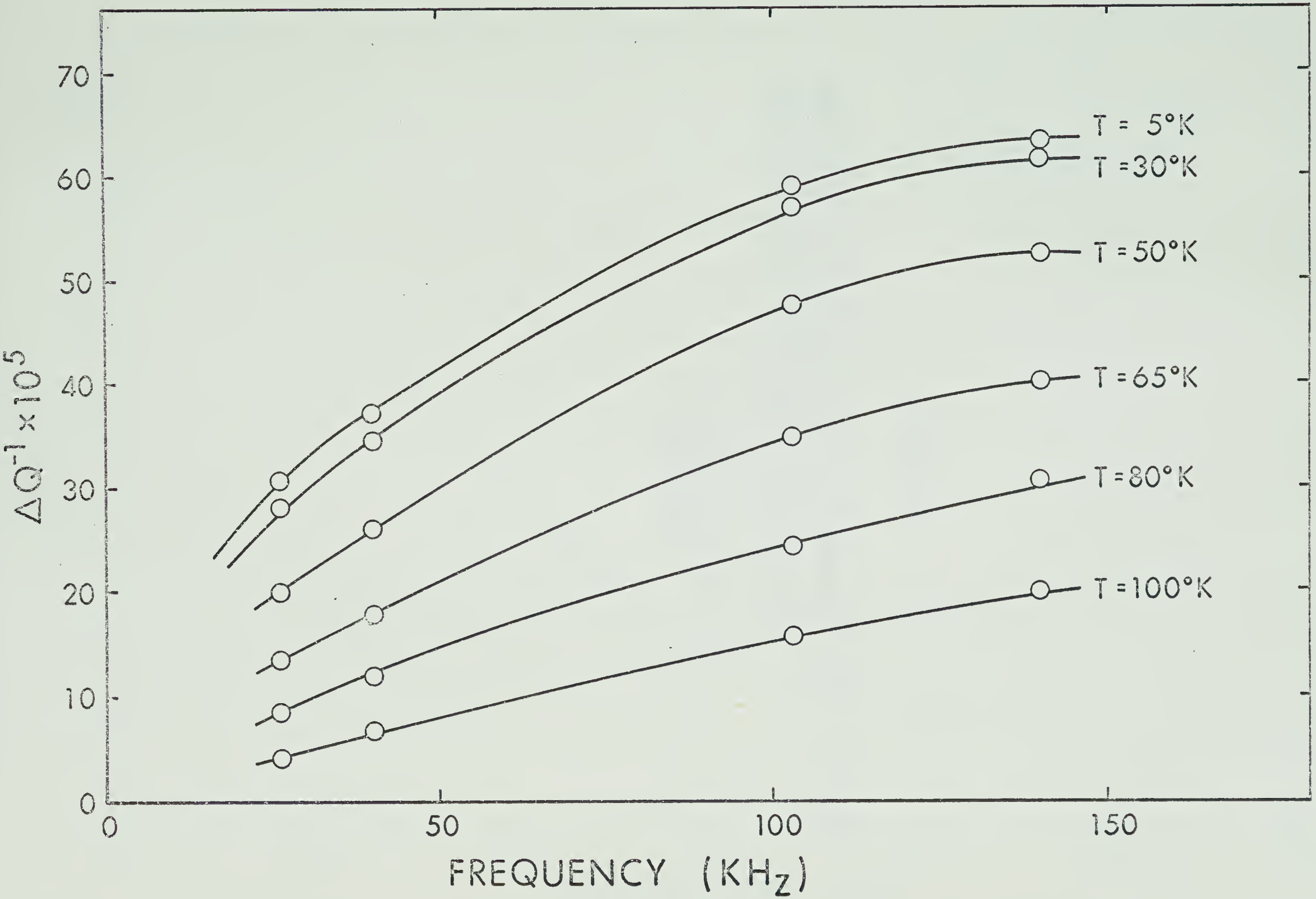
70
60
50
40
30
20
10
0
$\Delta Q^{-1} \times 10^5$
T = 5°K
T = 30°K
T = 50°K
T = 65°K
T = 80°K
T = 100°K
0
50
100
150
FREQUENCY (KH_Z)

Figure 4.3

The effect of a magnetic field on the dissipation in iron. The solid line represents data taken with no magnetic field.

- saturation field

- 600 oersted

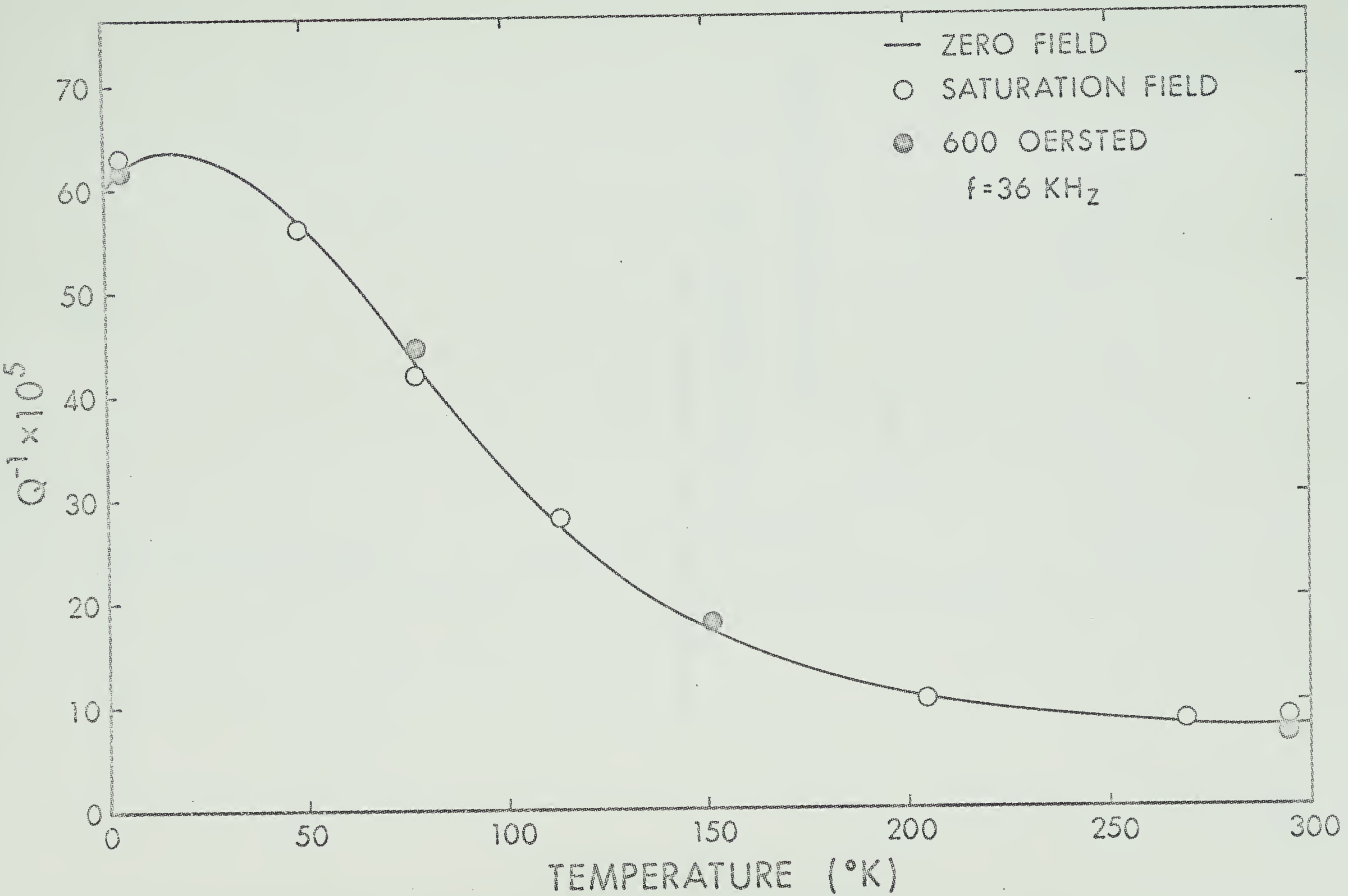
ZERO FIELD
SATURATION FIELD
600 OERSTED
f=36 KH2
70
60
50
40
30
20
10
0
0
50
100
150
200
250
300
σ1 x 10^5
TEMPERATURE (°K)

Figure 4.4

Damping of vibrations in nickel

● - as received condition

○ - after annealing 6 hours at 450° C in vacuum

NICKEL

● AS RECEIVED

○ AFTER ANNEALING

6 HRS. AT 450°C

$G_T A_T \times 10^5$

20

5

10

5

0

0

50

100

150

200

250

300

TEMPERATURE (°K)

The conclusion that must be drawn from this study is that the behavior of iron, with respect to vibration damping at low temperatures cannot be related to its magnetostrictive properties as was proposed by Heller.

In a further attempt to substantiate this statement, measurements of Q^{-1} were done on cobalt. The graph of figure 4.5 illustrates the results of these measurements on the sample as received from the supplier and figure 4.6 shows the variation of the resonant frequency with temperature. The large peak seen at about 120° K and its history dependence is believed to be due to the unstable hexagonal lattice of the cobalt. It was pointed out by Bozorth (1961, pp. 262) that the low temperature hexagonal phase is only approximately ideal close packed. This behavior is explained by the fact that the hexagonal phase is stable only at temperatures so low that the diffusion of atoms is extremely slow and they cannot form a perfect lattice after they have once been disrupted by the transformation. This transformation from cubic to hexagonal structure occurs at approximately 425° C.

The belief that the behavior shown in figure 4.5 and 4.6 was due to instability in the lattice was substantiated by measurements taken after the sample had been annealed above the transition temperature

Figure 4.5

The damping of vibrations in cobalts (as received condition) showing a hysteresis effect

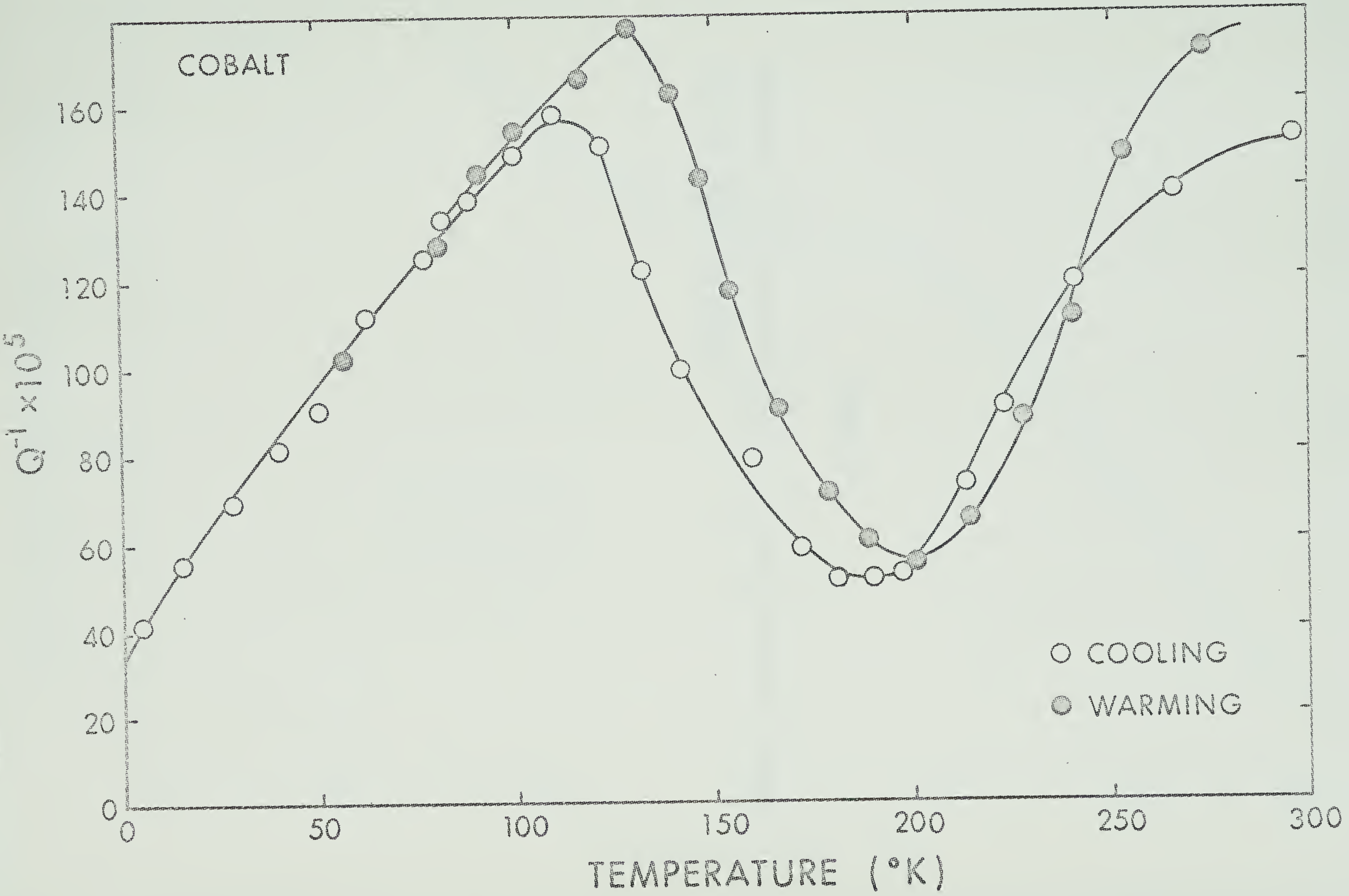
COBALT
160
140
120
100
80
60
40
20
0
0
50
100
150
200
250
300
TEMPERATURE (°K)
COOLING
WARMING

Figure 4.6

Variation of the resonant frequency of the cobalt sample with temperature (as received condition)

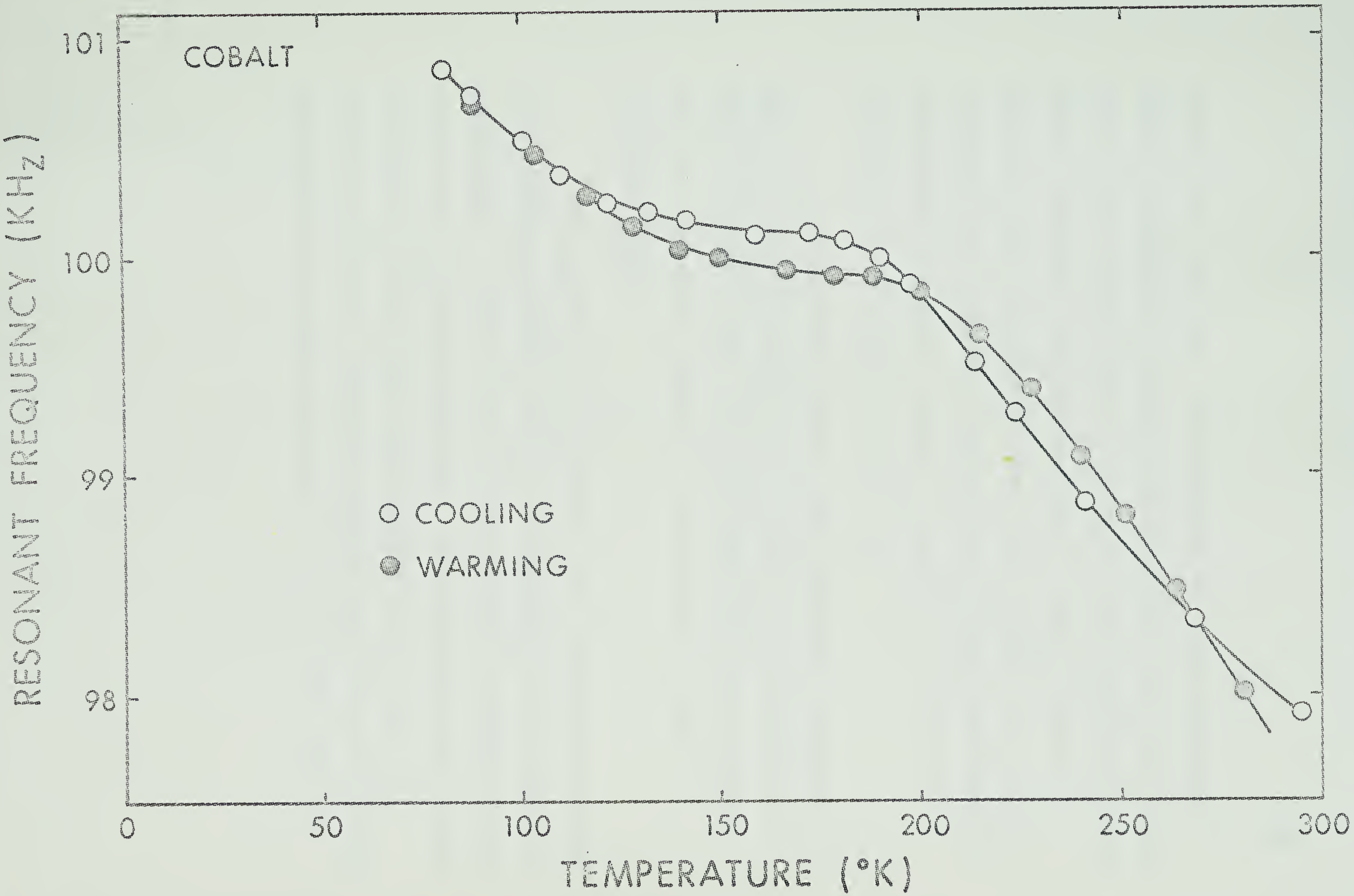
COBALT
O COOLING
WARMING
RESONANT FREQUENCY (KHz)
101
100
99
98
0
50
100
150
200
250
300
TEMPERATURE (°K)

at 550° C for three hours. The temperature was then slowly reduced through the transition temperature and maintained at 310° C for another three hours. From this point the cooling to room temperature took four hours. The results of these measurements are shown in figure 4.7. They do not show the hysteresis effect which had been seen previously. It should also be noted that after annealing treatments which involved quick cooling through the transition temperature measurements of Q^{-1} exhibited hysteresis similar to figure 4.5.

When the data in figure 4.7 are compared with the results for iron, it is seen that cobalt does not behave, at low temperature, in any way analogous to iron. This final result ties in with the belief that the ferromagnetic properties of iron are not the cause of its anomalous behavior.

The significant characteristic of the temperature dependence of the damping vibrations in iron is its resemblance to the electrical conductivity. A look at figure 4.8 shows that ΔQ^{-1} is directly proportional to the electrical conductivity. The conductivity curve shown is after White and Woods (1959) using 0.265 $\mu\Omega$ cm as the value of the residual resistivity. Measurements made on a bar of iron, cut from the same sheet as the samples and annealed at the same time, showed that

Figure 4.7

Damping (O) and resonant frequency (O) of cobalt after annealing and slow cooling through the cubic to hexagonal transition

COBALT

Q · X U D

RESONANT FREQUENCY (KHz)

30
25
20
15
10
5
0

14.0
13.9
13.8
13.7
13.6
27.0
26.8

0
50
100
150
200
250
300

TEMPERATURE (°K)

Figure 4.8

Comparison of the dissipation coefficient, ΔQ^{-1}, and the electrical conductivity of iron. The solid line represents the conductivity (after White and Woods, 1959) and the open circles are the measured values of ΔQ^{-1}.

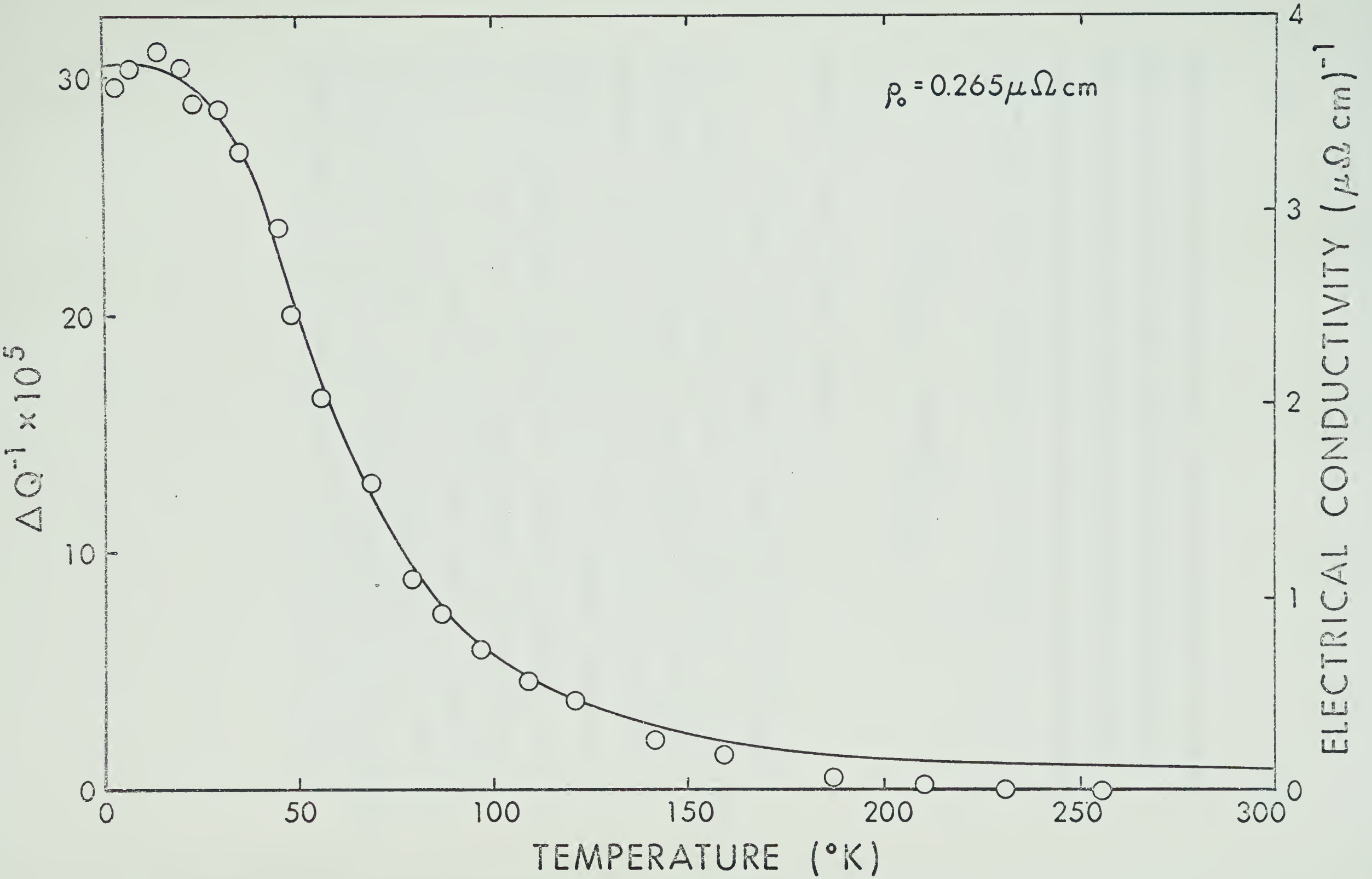
$\rho_o = 0.265 \mu\Omega\,cm$
$\Delta Q^{-1} \times 10^5$
ELECTRICAL CONDUCTIVITY $(\mu\Omega\,cm)^{-1}$
TEMPERATURE (°K)
0
10
20
30
0
1
2
3
4
0
50
100
150
200
250
300

this is not an unreasonable value. The above comparison was done for low frequency data (28 KHz). When this procedure was attempted for the data taken at a higher frequency, that is 140 KHz, there was a considerable deviation from direct proportionality with the electrical conductivity. This is illustrated by the following:

$$\left(\frac{Q^{-1}}{\sigma}\right)_{T=60^{\circ}K} = 1.4\left(\frac{Q^{-1}}{\sigma}\right)_{T=5^{\circ}K},$$

where σ is the electrical conductivity.

The fact that the damping of vibrations is proportional to the electrical conductivity, at least at low frequencies, indicates that the energy of the vibrations is being dissipated to the conduction electrons. It is now necessary to find the mechanism by which this dissipation occurs. The involvement of the conduction electrons hints at the electron-phonon interaction as a possible mechanism, however, as it was pointed out in a paper by Verdini (1962), the observed dissipation is a factor on the order of 10^3 greater than the one predicted by the free electron theory. It has been stated by Mason (1966, Vol IV B, pp.303) and in a paper by Jones and Raynes (1964) that the free electron theory underestimates the dissipation of elastic energy due to the

electron-phonon interaction in metals with a non-spherical Fermi surface such as iron, however, two orders of magnitude was the maximum discrepancy mentioned and this was for the high frequency range (approximately 1 GHz in molybdenum). The electron-phonon interaction theory also predicts that the dissipation should be directly proportional to the conductivity for the frequencies being studied here (Bhatia, 1967). This then does not explain the discrepancy seen at 140 KHz. It must be concluded from the above discussion that another mechanism is required to explain the anelastic behavior of iron at low temperatures.

In order to determine the nature of this mechanism it was necessary to know the influence of other parameters on the dissipation factor, Q^{-1}. It is known from the literature that the effect being studied is smaller in commercial grade iron than in the spec-pure grade used in this work (Verdini, 1962), and that the anomalous rise is lessened by the addition of hydrogen to the iron (Heller, 1961). It was also shown by Brunner (1960) that the amount of damping at low temperature is dependent on the dislocation density in the sample. The fact that the effect is smaller in hydrogen charged and commercial grade iron can be attributed to the smaller electrical conductivity due to impurity scattering. The dependence on the dislocation density cannot, however, be explained in this way. An increase in the dislocation density is

expected to reduce the conductivity and thereby reduce the low temperature damping. The measurements illustrated in figure 4.9 indicate that this is not the case. After a 5% compressional deformation of a sample, a change in the damping was observed. This change, however, instead of being uniquely negative as expected, was positive at 130 KHz and negative at 34 KHz. This result is thought to indicate that the dislocations play as direct a role in the damping mechanism as do the conduction electrons.

Theory of Acoustic Attenuation in Metals Due to Dislocations Damped by Electrons

A process by which dislocations, induced to move by the oscillating stress field in the sample, are damped by the conduction electrons is thought to provide a reasonable explanation for the observed phenomena. The theory governing this process was reviewed by Mason, in his book (1966, Vol IV B, pp. 310) and will be presented here.

It has been proposed by Koehler (1952) that many aspects of mechanical damping due to the presence of dislocations can be described by a model which assumes that the dislocation line segments act like a damped vibrating string, pinned at both ends. In this model, the equation of motion of the displacement, y, of a dislocation line in the

Figure 4.9

The effect of cold working on the dissipation in iron. The solid lines represent the measured values of Q^{-1} in an annealed sample and the circles represent measurements made on the same sample after a 5% deformation.

A - f = 34 KHz

B - f = 130 KHz

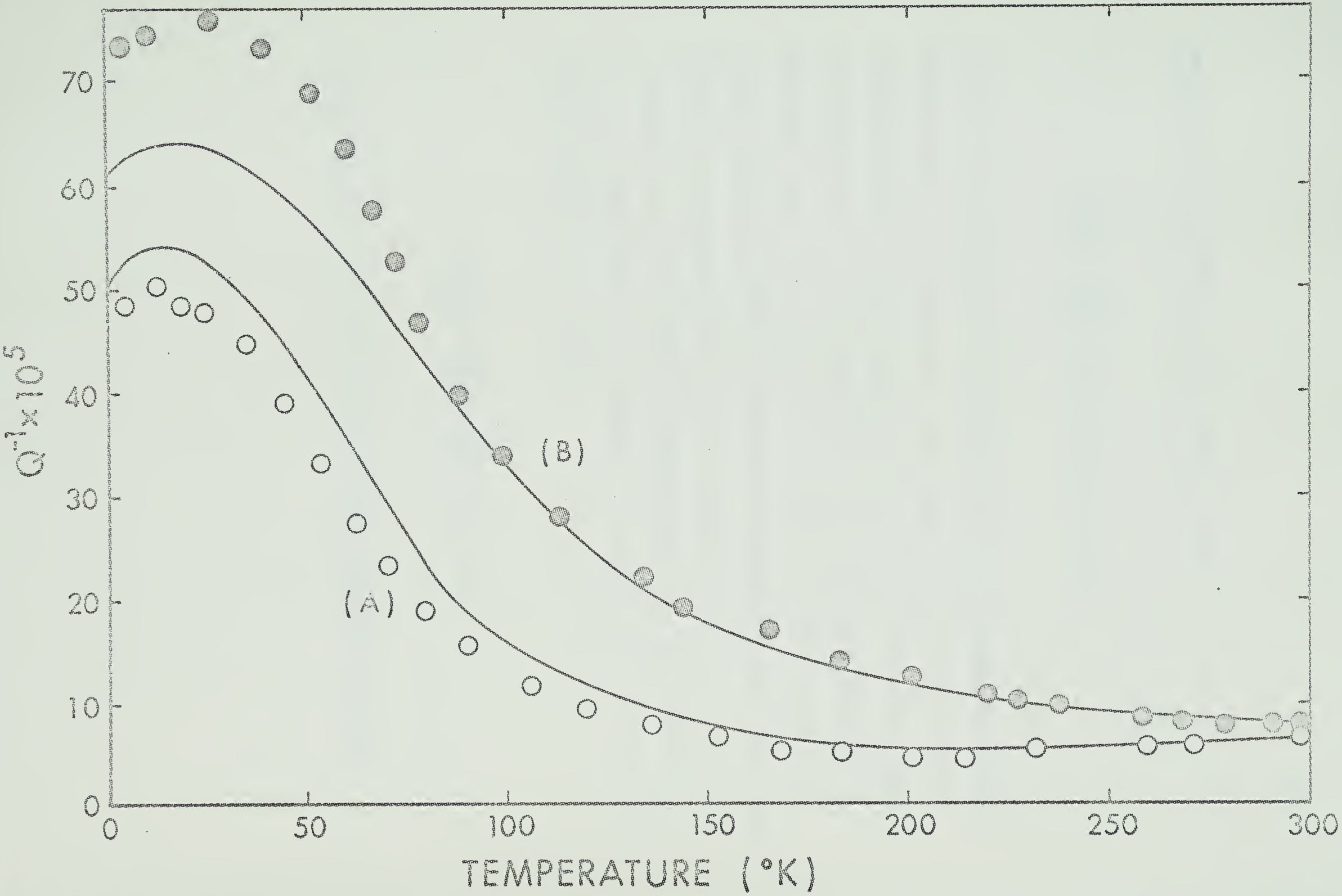
70
60
50
40
30
20
10
0
0
50
100
150
200
250
300
(B)
(A)
TEMPERATURE (°K)

presence of an oscillating stress field is then:

$$A \frac{\partial^2 y}{\partial t^2} - C \frac{\partial^2 y}{\partial x^2} = \text{force per unit length,}$$

where A is the effective line density and C is the tension in the dislocation line. The force given on the right hand side of the above equation includes the driving force of the stress field and the damping force which is, in this case, due to the conduction electrons. The force on the dislocation per unit length is taken to be σb (Cottrell, 1964, pp. 6), where σ is the shear stress component in the direction of the displacement and b is the Burgers vector of the dislocation. This model then assumes that the damping force is of the viscous type, that is, proportional to the velocity of the displacement and the equation of motion is then written:

$$A \frac{\partial^2 y}{\partial t^2} + B \frac{\partial y}{\partial t} - C \frac{\partial^2 y}{\partial x^2} = \sigma_o b \cos \omega t,$$

where B is the damping force per unit length, per unit velocity.

It was pointed out by Oen et al. (1960) that experimentally all types of dislocation damping show a broad maximum in their frequency dependence. It will be assumed here that the region of interest lies near to this maximum and that under these conditions, the motion of the dislocations is damping limited thereby making the inertia term negligible. Under this assumption the equation of motion must be written:

$$B \frac{\partial y}{\partial t} - C \frac{\partial^2 y}{\partial x^2} = \sigma_o b \cos \omega t, \qquad (4.1)$$

with the boundary conditions for a dislocation segment of length l being:

$$y(-\ell/2,t) = y(\ell/2,t) = 0. \qquad (4.2)$$

It is now necessary to evaluate the constant B for the case of electron damping of dislocations.

A dislocation is surrounded by a strain field and as it moves through the metal the strain at any point changes as a function of time. A changing strain indicates the atoms making up the metal are moving. The free electrons in the metal will then be imparted with this

same motion in order to establish current neutrality since the particles of the lattice are positively charged. These moving electrons can now be scattered by other electrons and thus the energy of the elastic vibrations can be dissipated. In order to develop a theory for this form of damping, the free electron gas is considered to be a viscous fluid of viscosity η.

In order to calculate the drag coefficient, B, for the moving dislocation segment it is necessary to know the form of the strain field around the dislocation. The simplest case to consider is the screw dislocation because of the symmetry of its strain field. The following treatment is after Cottrell (1953, pp. 36). If the z axis of a cylindrical coordinate system is chosen to be in the direction of the dislocation line, a screw dislocation is defined such that the displacement, ω, of the lattice from its ideal position has the form:

$$\omega = b(\theta/2\pi), \qquad (4.3)$$

where b is the magnitude of the Burgers vector and θ is zero at the slip plane. It follows from this that the only stress component present will be the shear, $\sigma_{\theta z}$, given by:

$$\sigma_{\theta z} = \frac{\mu}{r} \frac{\partial \omega}{\partial \theta} . \qquad (4.4)$$

Considering equation (4.3) this can be written:

$$\sigma_{\theta z} = \mu b/2\pi r, \qquad (4.5)$$

and the strain component will be given by:

$$S_{\theta z} = b/2\pi r , \qquad (4.6)$$

All other strain components of the dislocation field are zero.

When the above strain field moves through the viscous electron gas, energy is dissipated. This energy loss can be calculated for an elementary cylindrical volume from:

$$(T_{\theta z}\dot{S}_{\theta z})r\ dr\ d\theta\ dz = (\mu S_{\theta z}\dot{S}_{\theta z} + \eta \dot{S}^2_{\theta z})r\ dr\ d\theta\ dz , \qquad (4.8)$$

where $T_{\theta z}$ is the stress component containing an elastic term, $\sigma_{\theta z}$, and an anelastic term, $\eta\dot{S}_{\theta z}$, due to the viscous drag of the electrons.

It is now necessary to calculate $\dot{S}_{\theta z}$ for all points around a

dislocation moving with a velocity u, Considering a point initially at a distance r, from the dislocation line and at an angle θ from the direction of motion, the rate of change in $S_{\theta z}$ for a time interval dt is given by:

$$\frac{\Delta S_{\theta z}}{dt} = \frac{(b/2\pi)(\frac{1}{r_2} - \frac{1}{r_1})}{dt}, \qquad (4.9)$$

where r_2 is given by:

$$r_2 = r_1\left[1 - \frac{(\cos\theta)u\ dt}{r_1}\right].$$

The small limit of the above expression yields:

$$\dot{S}_{\theta z} = \frac{bu\cos\theta}{2\pi r^2}. \qquad (4.10)$$

The rate of energy dissipation per unit length of dislocation can now be calculated by substituting the expression for $\dot{S}_{\theta z}$ given by equation (4.10) and that of $S_{\theta z}$ given by equation (4.6) into equation (4.8) and integrating over a cylinder of unit length. This gives:

$$\dot{W} = \frac{b^2u^2\eta}{4\pi^2} \int_{a_o}^{\infty} r\, d\theta \int_0^{2\pi} \frac{\cos^2\theta}{r^4}\, d\theta = \frac{b^2u^2\eta}{8\pi a_o^2} \quad , \tag{4.11}$$

since the first term in (4.8) is the elastic term and does not contribute to the integral. In order to evaluate the drag coefficient B, the energy dissipated by the strain field must be equated to the work done by the force per unit length, F, applied to the dislocation. In the coordinate system used above,

$$F = T_{13}b \ , \tag{4.12}$$

and the velocity u, attained by the dislocation, is given by:

$$\frac{F}{B} = u \ . \tag{4.13}$$

It is seen from equations (4.11), (4.12) and (4.13) that,

$$\dot{W} = u^2 B = \frac{b^2u^2\eta}{8\pi a_o^2} \ , \tag{4.14}$$

hence:

$$B = \frac{b^2 \eta}{8\pi a_o^2} . \qquad (4.15)$$

The quantity a_o appearing in equation (4.15) and in equation (4.11) is the smallest radius around the dislocation line for which the strain field is elastic. Inside this radius the motion of the dislocation is discontinuous and the damping due to the viscosity of the conduction electrons is assumed to be zero. The dissipation of energy via acoustic radiation due to the discontinuous motion of the atoms within this radius is neglected in the theory. A value of 3/4 b has been given for a_o by Cottrell (1953, pp. 39). A completely analogous treatment of edge dislocations (Mason 1966, Vol IV A, pp. 313) leads to a similar expression for the damping constant of edge dislocations. In this case:

$$B = \frac{0.75\, b^2 \eta}{8\pi(1-\sigma_p)^2 a_o^2} , \qquad (4.16)$$

where σ_p is the Poisson's ratio.

The viscosity η, of the electron gas, is evaluated by assuming it to be analogous to a classical viscous fluid. It is well known

for this case that,

$$\eta = \frac{N' m \bar{\ell} V_{rms}}{3}, \tag{4.17}$$

where N' is the free electron density, m is the mass of the electrons, $\bar{\ell}$ is the mean free path between collisions and V_{rms} is the root mean square velocity. In the case of a metal with a spherical Fermi surface, V_{rms} can be replaced by 3/5 of the Fermi velocity v_F:

$$\eta = \frac{N' m v_F \bar{\ell}}{5}. \tag{4.18}$$

When the mean free path and the Fermi velocity are expressed in terms of the electrical conductivity, σ, and the free electron density (Kittel, 1956, chapter 10), it is found that:

$$\eta = \frac{\hbar^2 (3\pi^2 N')^{3/2} \sigma}{5e^2}, \tag{4.19}$$

where e is the electronic charge and $\hbar$ is Planck's constant divided by 2π.

The constant C in equation (4.1), that is the effective tension in the moving dislocation line, remains to be evaluated. It has been stated by Cottrell (1964, pp. 53) that an acceptable form for the tension is given by the equation:

$$C = \frac{\mu b^2}{2} , \tag{4.20}$$

where μ is the shear modulus of the metal.

The equation of motion of the pinned dislocation segments,

$$B \frac{\partial y}{\partial t} - C \frac{\partial^2 y}{\partial x^2} = \sigma_o b \cos \omega t , \tag{4.1}$$

is now completely known since the constants B and C can be evaluated using equations (4.15), (4.16), (4.19) and (4.20). In their paper, Cen et al. (1960) gave the steady state solution of equation (4.1) as:

$$y(x,t) = \frac{\sigma_o b}{\omega B} \left\{ \sin \omega t \left[1 - \frac{\cosh kx \cos kx \cosh(\frac{k\ell}{2}) \cos(\frac{k\ell}{2})}{\cosh^2(\frac{k\ell}{2}) - \sin^2(\frac{k\ell}{2})} \right. \right.$$

$$+\frac{\sinh kx \sin kx \sinh(\frac{k\ell}{2})\sin(\frac{k\ell}{2})}{\cosh^2(\frac{k\ell}{2}) - \sin^2(\frac{k\ell}{2})}\Bigg]$$

$$+\cos \omega t\Bigg[\frac{\cosh kx \cos kx \sinh(\frac{k\ell}{2})\sin(\frac{k\ell}{2})}{\cosh^2(\frac{k\ell}{2}) - \sin^2(\frac{k\ell}{2})}$$

$$-\frac{\sinh kx \sin kx \cosh(\frac{k\ell}{2})\cos(\frac{k\ell}{2})}{\cosh^2(\frac{k\ell}{2}) - \sin^2(\frac{k\ell}{2})}\Bigg]\Bigg\}\,, \qquad (4.21)$$

where $k^2 = \omega B/2C$. Expressed as the sum of harmonics, the displacement is,

$$y(x,t) = \frac{4\sigma_o b}{\pi}\sum_{n=0}^{\infty}\left\{\frac{\sin\left[a_n(x+\ell/2)\right]}{2n+1}\left(\frac{a_n^2 C\cos\omega t}{a_n^4C^2+\omega^2B^2} + \frac{\omega B\sin\omega t}{a_n^4C^2+\omega^2B^2}\right)\right\}\,, \qquad (4.22)$$

where $a_n = (2n+1)\pi/\ell$. Using equation (2.21) the dissipation factor, Q^{-1}, is calculated from:

$$Q^{-1} = \frac{1}{\pi}\,\frac{\int_o^{\infty} E(\ell)N(\ell)\,d\ell}{\sigma_o^2/\mu}\,, \qquad (4.23)$$

where $N(\ell)\, d\ell$ is the number of dislocation segments per unit volume, with the distance between their pinning points being between ℓ and $\ell + d\ell$. The energy loss per cycle for one dislocation segment of length ℓ is given by $E(\ell)$ which is calculated from:

$$E(\ell) = \int_{-\ell/2}^{\ell/2} dx \int_{0}^{2\pi} \sigma_o b \cos \omega t \, \frac{dy(x,t)}{dt} \, dt . \qquad (4.24)$$

Assuming that the distance between pinning points on the dislocations is distributed exponentially about a mean value, ℓ_o (Koehler, 1952), that is

$$N(\ell) = \frac{L}{\ell_o^2} e^{-\ell/\ell_o}, \qquad (4.25)$$

where L is the total length of dislocations per unit volume, then the value of Q^{-1} is given by

$$\frac{Q^{-1}}{L\ell_o^2} = \frac{1}{(k\ell_o)^3} \int_0^\infty \left[k\ell_o x - \left(\frac{\sinh k\ell_o x + \sin k\ell_o x}{\cosh k\ell_o x + \cos k\ell_o x} \right) \right] e^{-x} \, dx . \qquad (4.26)$$

In order to account for the fact that the applied stress is not always of the form and direction given in equation (4.12), it is necessary to introduce an orientation factor R (Alers and Thompson, 1961) so that equation (4.26) now reads:

$$\frac{Q^{-1}}{NR\ell_o^2} = \frac{1}{(k\ell_o)^3} \int_0^\infty \left[k\ell_o x - \left(\frac{\sinh k\ell_o x + \sin k\ell_o x}{\cosh k\ell_o x + \cos k\ell_o x} \right) \right] e^{-x}\, dx \,. \qquad (4.27)$$

The range of R is given by the above authors as 0.08 to 0.2. The dissipation coefficient, Q^{-1}, as given by equation (4.27) has the amplitude independence that is required by the experimental results. The asymptotic behavior of the above equation, for low frequencies, is given by:

$$Q^{-1} = 4\, NR\ell_o^2 \frac{\omega}{\omega_o} \,, \quad (\omega \ll \omega_o) \qquad (4.28)$$

and for high frequencies by:

$$Q^{-1} = NR\ell_o^2 \frac{\omega_o}{\omega} \,, \quad (\omega \gg \omega_o) \qquad (4.29)$$

where ω_o is given by:

$$\omega_o = \frac{2C}{B\ell_o^2} . \qquad (4.30)$$

From equations (4.15), (4.16) and (4.19) it is seen that ω_o must be inversely porportional to the electrical conductivity. The dissipation of elastic energy at low frequencies, as indicated in equation (4.28), is directly proportional to the electrical conductivity. This is in agreement with the experimental results which are illustrated in figure 4.8. The deviation from this direct proportionality, seen at higher frequencies, is also expected from the theory. The integral of equation (3.26) has been calculated numerically (Cen et al., 1960) for the frequency range around ω_o. The result of this calculation is the universal curve shown in figure 4.10. It was possible to fit the experimental results illustrated in figure 4.2 to this curve. The best agreement between theory and experiment, as illustrated in figure 4.11, was achieved by using a value of 1.83×10^{-3} for the product $NR\ell_o^2$ and a value of ω_o which was temperature dependent. Figure 4.12 is a plot of ω_o^{-1} versus temperature as used in this fit. It is now necessary to compare these parameters with their accepted values in iron. According to Van Buren (1961, pp. 328), a reasonable value for the number of dislocations cutting a surface of unit area in a well annealled metal is 10^7 cm^{-2}.

Figure 4.10

The frequency of Q^{-1} for dislocation damping by electrons (after Oen et al., 1960)

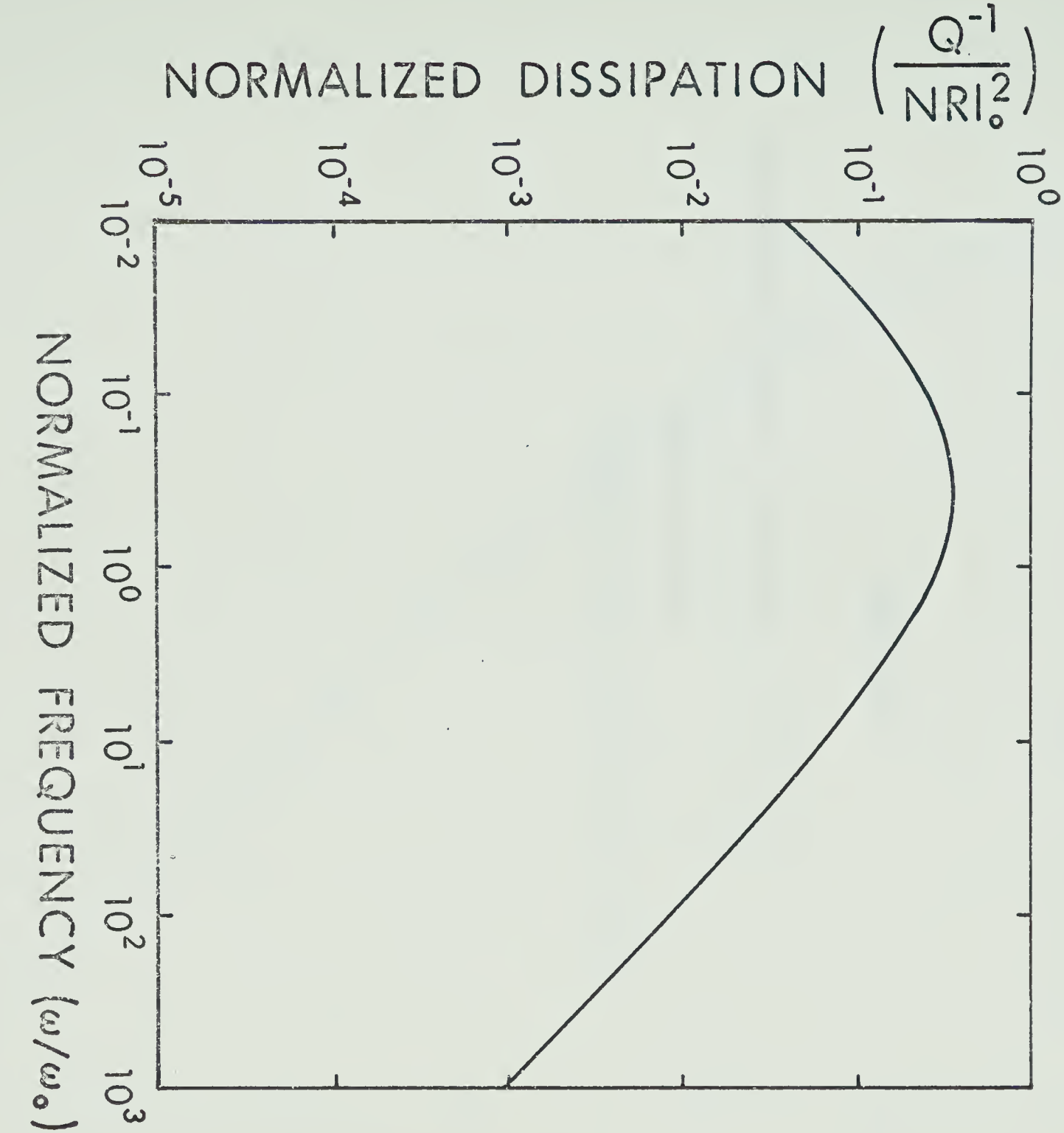
NORMALIZED DISSIPATION $\left(\frac{Q^{-1}}{NRI_o^2}\right)$
10^{-5}
10^{-4}
10^{-3}
10^{-2}
10^{-1}
10^{0}
NORMALIZED FREQUENCY (ω/ω_o)
10^{-2}
10^{-1}
10^{0}
10^{1}
10^{2}
10^{3}

Figure 4.11

The normalized frequency dependence of Q^{-1} in iron

Observed results

Theoretical curve after Oen et al. (1960)

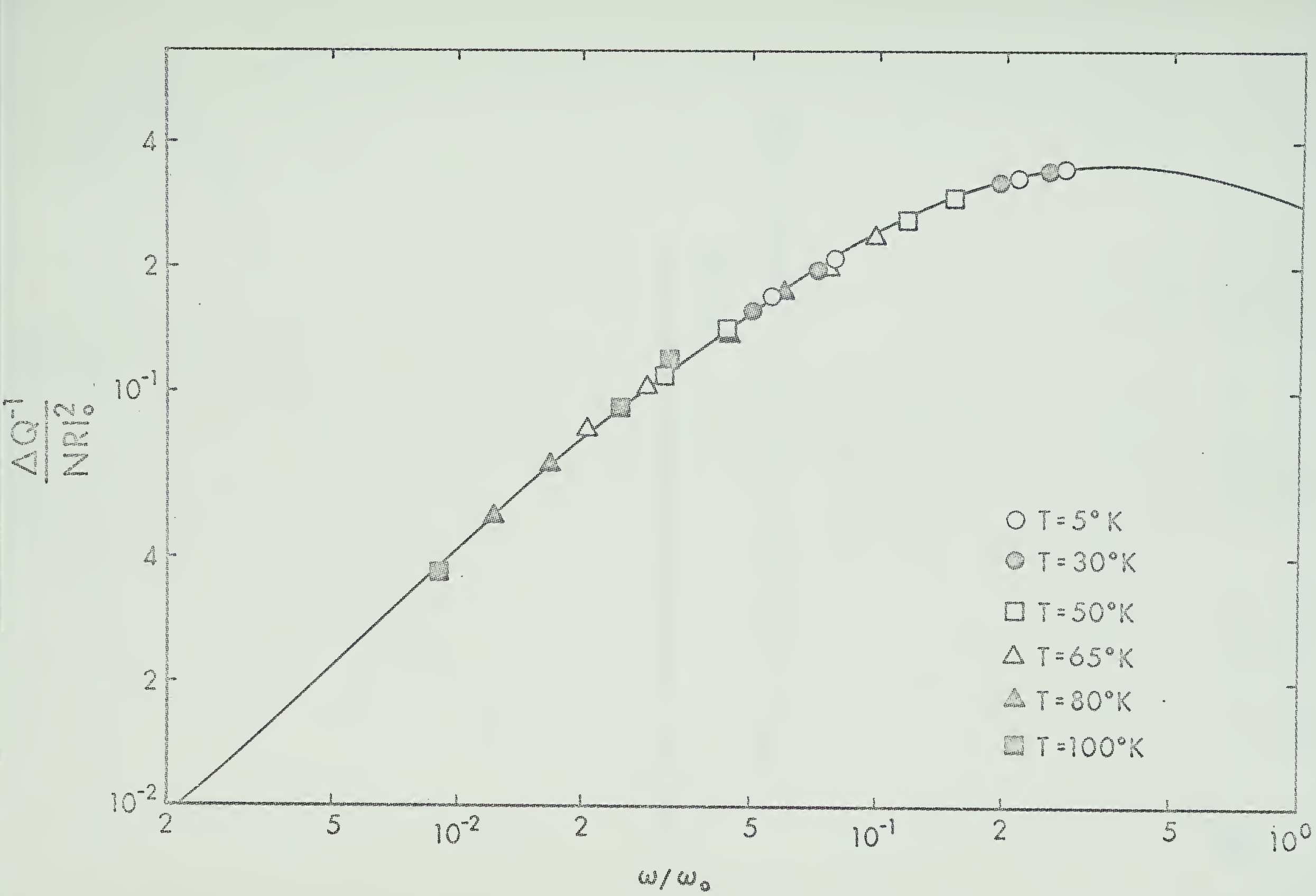
ΔG^{-1}
N_{P2}
10^{-1}
4
2
4
2
10^{-2}
2
5
10^{-2}
2
5
10^{-1}
2
5
10^{0}
ω/ω_0
O T = 5° K
T = 30° K
T = 50° K
T = 65° K
T = 80° K
T = 100° K

Figure 4.12

ω_o^{-1} vs. temperature as used to plot observed results in figure 4.11

O - ω_o^{-1}

——— - electrical conductivity after White and Woods (1959)

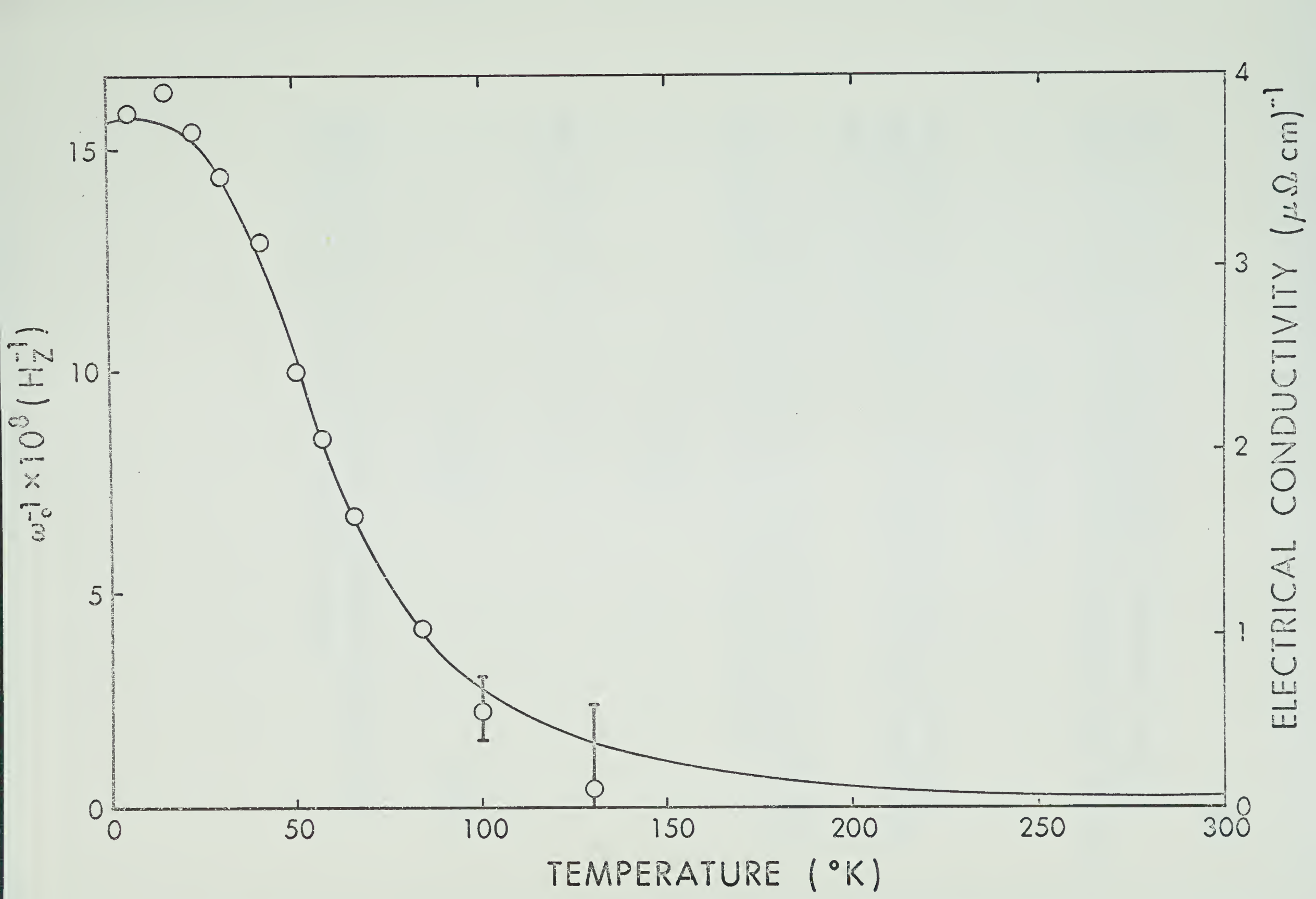
$\omega_c^{-1} \times 10^8$ (Hz^{-1})
0
5
10
15
0
50
100
150
200
250
300
TEMPERATURE (°K)
ELECTRICAL CONDUCTIVITY ($\mu\Omega$ cm)$^{-1}$
0
1
2
3
4

This is equivalent to N, the total length of dislocations per unit volume. If a value of 0.1 is assumed for the orientation factor R, since:

$$NR\ell_o^2 = 1.83 \times 10^{-3} ,$$

it is found that ℓ_o must have a value of 4.3×10^{-5} cm. This is considered to be a reasonable average length for dislocations (Mason, 1966, Vol IV A, pp. 320).

In order to compare the experimental values of ω_o with theory, it is necessary to develop further equation (4.30) which reads:

$$\omega_o = \frac{2C}{B\ell_o^2} .$$

From equation (4.20) it is seen that:

$$\omega_o = \frac{\mu b^2}{B\ell_o^2} . \qquad (4.31)$$

If it is assumed that B is given by its expression in equation (4.16) for edge dislocations, equation (4.31) can be written:

$$\omega_o = \frac{8\pi\mu(1-\sigma_p)^2 a_o^2}{0.75\, l_o^2 \eta} \,. \qquad (4.32)$$

Using equation (4.19) it can be seen that:

$$\omega_o = 17.7 \frac{(1-\sigma_p)^2 a_o e^2}{N'^{2/3} l_o^2 h^2 \sigma} \,. \qquad (4.33)$$

Assuming that the effective density of free electron, N', is independent of temperature and since the elastic modulii are very nearly independent of temperature (Bhatia, 1967), it is found that ω_o should be inversely proportional to the electrical conductivity σ. The experimental values of ω_o were compared with the electrical conductivity in figure 4.2 and are seen to be in very good agreement with this finding. Although the temperature dependence of ω_o found experimentally is in agreement with equation (4.33), there is a discrepancy in the magnitude of this parameter. In order to evaluate ω_o from equation (4.33), a value of 0.2 free electrons per atom was used to arrive at N' (Mott and Jones, 1958, pp. 222). The dislocations were assumed to all be of the unit type giving a_o a value of approximately 10^{-8} cm ($a_o \approx 3/4$ b). This led to:

$$(\omega_o \sigma)_{theory} = 9 \times 10^8 \ (\mu\Omega \text{ cm sec})^{-1}. \qquad (4.34)$$

From figure (4.12) it is seen that:

$$(\omega_o \sigma)_{exp.} = 2.45 \times 10^7 \ (\mu\Omega \text{ cm sec})^{-1}. \qquad (4.35)$$

It is believed that the discrepancy between equations (4.34) and (4.35) can be explained through either of two weaknesses in the theory. These weaknesses lie in the calculation of the damping constant B and in the assumed distribution of dislocation lengths of equation (4.25). Equations (4.15) and (4.16) are two expressions for the constant B, one for screw dislocations and the other for edge dislocations. Although both of these expressions give the required temperature dependence of ω_o when substituted into equation (4.31), that of equation (4.16), giving the damping constant of edge dislocations was used to arrive at the value of ω_o in equation (4.34)., the reason being that better agreement was obtained in this way between expressions (4.34) and (4.35). It is possible that a third type of dislocation is responsible for the observed behavior. In applying the damping constant of edge dislocations to equation (4.31) it was assumed that all the dislocations were of the unit type. This was not done in consideration of the properties of iron

but only to facilitate calculations. This assumption fixed the value of a_o at 10^{-8} cm. It is very probable that the Burgers vectors of the dislocations in iron have a range of values and it is possible that because of this the parameter a_o has a smaller effective value than the one assumed above. This would lead to a smaller theoretical value for ω_o.

With reference to the distribution of the distance between pinning points assumed in equation (4.25), it has been shown by Cen et al. (1960) that if one assumes a delta function distribution for this length that the peak shown in figure 4.10 is shifted to a larger value of ω/ω_o. The general characteristics of the temperature and frequency dependence of Q^{-1}, however, remain much the same. In this case, a fit of the experimental data like that of figure 4.11 would give an even smaller experimental value to ω_o. The delta function distribution of the distance between pinning point must be discounted because of their random nature, however, a distribution which would produce a shift of the peak in the opposite direction cannot be ignored. It is well known that the dislocation structure of iron is peculiar to this metal as evidenced by the fact that no Bordoni peak has yet been observed in it. This may also explain the fact that, in metals which have similar crystal and electronic structures to that of iron such as niobium and tantalum, there have been

no observations of this type of damping. In summary, it is thought the fact that ω_o, as measured in iron, is much smaller than expected can be explained by a peculiar dislocation structure in iron.

This small value of ω_o provides an explanation for measurements done in the megacycle frequency range by Verdini (private communication). During the course of this work the type of damping which occurs at lower frequency was not observed. For this frequency range it is expected from equation (4.29) that Q^{-1} will be directly proportional to the electrical resistivity. The behavior would be almost indistinguishable from the background damping due to dislocation-phonon and dislocation-dislocation interactions.

CHAPTER V

CONCLUSIONS AND SUGGESTIONS FOR FURTHER WORK

The anomalous behavior of vibration damping in iron, at low temperatures, has been studied experimentally. The proportionality of the dissipation coefficient, Q^{-1}, to the electrical conductivity and its dependence on the density of dislocations led to an interpretation of this effect as being due to the damping of the moving dislocation lines in the sample by the conduction electrons. The theory of this damping mechanism is presented in the text and good agreement is shown to exist between theory and experiment in the form of the temperature and frequency dependence of Q^{-1}. The theory presented indicates that a maximum value of Q^{-1} should occur at a certain frequency. The value of this frequency determined from the experimental results is much smaller than that predicted by the theory. It is thought that this discrepancy can be explained by the fact that the theory does not take into account the possible existence of a dislocation structure which is peculiar to iron.

In order to clarify the existing situation, a series of experiments have been planned for the future.

(1) A study of the effect of γ irradiation on the dissipation coefficient Q^{-1} would provide a controlled method of studying the effect of changes in the dislocation structure of iron. In complement to this a systematic study of the effect of various annealing treatments and cold-working could provide new experimental information. Modification of the existing equipment is being considered in order to allow measurements of both Q^{-1} and the electrical resistivity in the same sample. Any changes in the resistivity due to the above treatments could then be taken into account when studying the dislocation structure. This is necessary since both of these properties effect the value of Q^{-1}.

(2) Since a sample vibrating in its flexural mode experiences both shear and longitudinal stress, it is not known whether vibrations which contain only pure shear or pure longitudinal stresses are damped in the same way. For this reason, measurement of Q^{-1} for extensional and torsional vibrations in a bar shaped sample of iron are planned for a wide range of frequencies.

During the course of the present research the dissipation factor, Q^{-1}, was measured in cobalt and nickel. These two metals did not exhibit the behavior seen in iron. The measurements on cobalt, however, did show evidence of the unstable low temperature hexagonal phase of this metal.

REFERENCES

Alers, G., Thomson, D.O. (1961) J. Appl. Phys., 32 , 283.

Bhatia, A.B., (1967) "Ultrasonic Absorption, Oxford, London.

Bordoni, P.G., Nuovo, M. and Verdini, L., (1959) Nuovo Cimento, 14, 2, 273.

Bordoni, P.G., (1961) "Progress Report to U.S. Department of the Army". unpublished.

Bozorth, R.M., (1951) "Ferromagnetism", Van Nostrand, New York.

Bruner, L.S., (1959) Phys. Rev., 118, 399.

Cottrell, A.H., (1953) "Dislocations and Plastic Flow Crystals", Oxford, London.

Cottrell, A.H., (1964) "Theory of Crystal Dislocations", Gordon and Breach, New York.

Heller, W. R., (1961) Acta. Met., 9, 600.

Jones, C.K. and Raynes, J., (1964) Phys. letters, 13, 282.

Kittel, C., (1956) "Introduction to Solid State Physics", Wiley, New York.

Koehler, J. S., (1952) "Imperfections in Nearly Perfect Crystals", Wiley, New York.

Mason, W. P., (1966) "Physical Acoustics", Academic Press, New York.

Mott, N. F. and Jones, H., (1958) "The Theory of the Properties of Metals and Alloys", Dover, New York.

Nuovo, M., (1961) Ric. Sci., 31 (II-A), 212-243.

Oen, O.S., Holmes, D.K. and Robinson, M.T., (1960) U.S. Atomic Energy Commission Report ORNL-3017, p.3.

Powell, R.L., Bunch, M.D. and Corruccini, R.J., (1961) Cryogenics, 1, 139.

Van Buren, H.G., (1961) "Imperfections in Crystals", North Holland, Amsterdam.

Verdini, L., (1962) Nuovo Cimento Suppl., 25, 2, 258.

White, G.K. and Woods, S.B., (1959) Phil. Trans. A, 251, 274.

Zener, C. (1948) "Elasticity and Anelasticity in Metals", Chicago University, Chicago.

APPENDIX I

PARAMETERS FOR FLEXURAL VIBRATIONS IN THIN PLATES*

For a circular plate of radius a and thickness h, the frequency of the normal flexural modes of vibration are given by

$$f_{m,n} = \alpha_{m,n} \frac{h}{a^2} \left(\frac{E}{\rho(1 - \sigma_p^2)} \right)^{1/2} \qquad \text{(I-1)}$$

where E is Young's modulus, σ_p is the Poisson's ratio and ρ is the density of the material. The constants, $\alpha_{m,n}$ are the eigenvalues of the modes with m nodal circles and n nodal diameters. The values of $\alpha_{m,n}$ are given in the following table:

m	n = 0	n = 1	n = 2	n = 3
0	-	-	0.241	0.562
1	0.417	0.943	1.619	2.431
2	1.770	2.750	-	-

(I-2)

* After Nuovo (1961)

Since the force of the electrode on the sample was applied almost uniformly over a circular area, only modes with this symmetry were used for measurements, that is modes with no nodal diameters. The radius of the nodal diameters for the first two such modes is given by:

$$r_{1,0} = 0.678a; \quad \begin{cases} r'_{2,0} = 0.392a \\ r''_{2,0} = 0.842a \end{cases} \qquad \text{(I-3)}$$

When running in the second mode the mounting pins were placed on the nodal circle of radius $r''_{2,0}$ since it is larger than $r'_{2,0}$ and affords better support for the sample.

APPENDIX II

PHYSICAL CHARACTERISTICS OF SAMPLES

IRON (Johnson Matthey spectrographically standardized)

A. Spectral Analysis

Element	Quantity present (ppm)
Silicon	8
Manganese	3
Nickel	3
Copper	2
Magnesium	1
Silver	less than 1

B. (1) Figure 4.1

Sample #1: diameter - 30 mm

thickness - 30 mm

Sample #2: diameter - 25 mm

thickness - 3 mm

(2) Figures 4.3 and 4.9

Before compression: diameter - 25 mm

thickness - 2.6 mm

After compression: diameter - 25 mm
(using force of thickness - 2.5 mm (irregular)
25,000 lbs.)

NICKEL (source unknown)

Figure 4.4: diameter - 36 mm
thickness - 5 mm

COBALT (Johnson Matthey spectrographically standardized)

A. Spectral Analysis

Impurity content found to be very similar to that of iron, that is less than 20 parts per million.

B. Figure 4.5, 4.6 and 4.7: diameter - 30 mm
thickness - 5 mm